

Iron and Cobalt Diazoalkane Complexes Supported by β -Diketiminato Ligands: A Synthetic, Spectroscopic, and Computational Investigation

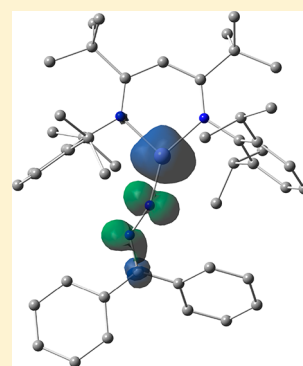
Simon J. Bonyhady,[†] Daniel E. DeRoshia,[†] Javier Vela,^{‡,§} David J. Vinyard,^{†,||} Ryan E. Cowley,^{‡,||} Brandon Q. Mercado,[†] William W. Brennessel,^{‡,||} and Patrick L. Holland^{*,†,||}

[†]Department of Chemistry, Yale University, 225 Prospect Street, New Haven, Connecticut 06520, United States

[‡]Department of Chemistry, University of Rochester, 120 Trustee Road, Rochester, New York 14627, United States

Supporting Information

ABSTRACT: Diazoalkanes are interesting redox-active ligands and also precursors to carbene fragments. We describe a systematic study of the binding and electronic structure of diphenyldiazomethane complexes of β -diketiminato supported iron and cobalt, which span a range of formal d-electron counts of 7–9. In end-on diazoalkane complexes of formally monovalent three-coordinate transition metals, the electronic structures are best described as having the metal in the +2 oxidation state with an antiferromagnetically coupled radical anion diazoalkane as shown by crystallography, spectroscopy, and computations. A formally zerovalent cobalt complex has different structures depending on whether potassium binds; potassium binding gives transfer of two electrons into the η^2 -diazoalkane, but the removal of the potassium with crown ether leads to a form with only one electron transferred into an η^1 -diazoalkane. These results demonstrate the influence of potassium binding and metal oxidation state on the charge localization in the diazoalkane complexes. Interestingly, none of these reduced complexes yield carbene fragments, but the new cobalt(II) complex $L^{\text{tBu}}\text{CoPF}_6$ (L^{tBu} = bulky β -diketiminato) does catalyze the formation of an azine from its cognate diazoalkane, suggesting N_2 loss and transient carbene formation.



INTRODUCTION

Transition metal diazoalkane complexes have rich coordination chemistry and reactivity.^{1,2} Continued interest is based on the redox-active nature of the diazoalkane which can accept electrons from the metal, and also their utility as atom economical precursors to carbene complexes that are potential catalysts for olefin metathesis or alkene cyclopropanation.³ The catalytic potential of inexpensive first row transition metal complexes makes them especially attractive for catalysis, but there are relatively few structurally characterized carbene complexes of the electrophilic late first-row transition metals Mn, Fe, Co, Ni, and Cu.⁴ There are a few systems for which both the diazoalkane adduct and the corresponding carbene complex have been synthesized and structurally characterized,⁵ and conversion from the former to the latter may be brought about by photolysis,^{5d} thermolysis^{5a,c} or Lewis acid catalysis.^{5b} There are also systems in which carbene-like reactivity has been observed from the diazoalkane adduct when it is exposed to the aforementioned conditions, although the reactive species was not isolated.⁶ However, there is a lack of guiding principles for predicting whether carbene formation will be possible from a given diazoalkane complex. This situation motivates the study of the electronic structure of diazoalkane complexes as a guide to their reactivity.

Two descriptions of diazoalkane complexes are predominant in the literature (Figure 1).¹ First, diazoalkane adducts, I, featuring linear M–N–N and N–N–C angles, generally

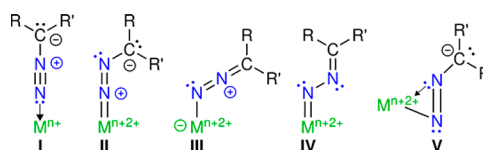


Figure 1. Lewis structures of transition metal diazoalkane complexes: neutral adduct I; hydrazonido ligands II, III, and IV; side-bound hydrazonido ligand V.

suggest that no reduction of the diazoalkane has occurred upon coordination. Second, formal hydrazonido(2-) ligands, II–V, in which the diazoalkane has been reduced by two electrons, feature M–N–N and/or N–N–C angles near 120°. The further reactivity of these systems, such as N–N⁷ and C–N³ cleavage, is inextricably linked with charge movement within the N_2C moiety. Therefore, it is of interest to identify the systems in which this change of electronic structure can be modulated rationally.

More recently an intermediate bonding situation has been discovered, in which the diazoalkane accepts only one electron. Although single electron reduction of diazofluorene with sodium metal was reported as early as the 1960s,⁸ ligand radical character in transition metal or f-block metal diazoalkane complexes is rarely identified.⁹ We have reported

Received: February 21, 2018

the cobalt diazoalkane complex $L^{tBu}Co(\eta^1-N_2CPh_2)$, **1-Co** ($L^{tBu} = [(\text{Dipp})NC(tBu)_2CH]^-$ where $\text{Dipp} = 2,6\text{-}iPr_2C_6H_3$),¹⁰ which X-ray crystallographic and computational studies showed was best described as high-spin cobalt(II) antiferromagnetically coupled to the radical anion of diphenyldiazomethane.

Given the paucity of diazoalkane complexes in which single electron reduction of the diazoalkane moiety has been studied, the effect of single electron transfers on electronic structure and reactivity is poorly understood. Due to the accessibility of late transition metal complexes with a variety of metals and oxidation states within β -diketiminato frameworks,¹¹ these ligands provide a useful platform for an investigation into the effects of transition metal electronic configuration on the coordinated diazoalkane moiety. Herein, we report the effect of metal oxidation state on diazoalkane binding and reactivity, while limiting the supporting ligand framework to a single β -diketiminato. This study spans a range of total electron counts, and with varied Lewis acid (potassium) coordination. We show that the number of electrons in the frontier orbitals has a marked influence on the diazoalkane binding mode, ligand redox level, and reactivity.

EXPERIMENTAL SECTION

General. All manipulations were performed under a nitrogen atmosphere (or argon atmosphere where specified) by Schlenk techniques or in an M. Braun glovebox maintained at or below 1 ppm of O_2 . Glassware was dried at 150 °C overnight, and Celite was dried overnight at 200 °C under vacuum. Pentane, hexane, benzene, diethyl ether, and toluene were purified by passage through activated alumina and Q5 columns from Glass Contour Co, under Ar. THF was distilled under argon from a potassium benzophenone ketyl solution. All solvents were stored over 4 Å molecular sieves and passed through a plug of activated alumina immediately prior to use. Benzene- d_6 was dried over activated alumina and stored over 4 Å molecular sieves. Silver hexafluorophosphate (99%) was purchased from Strem Chemicals and used as received.

The following starting materials were prepared according to literature procedures and stored at -40 °C under an inert atmosphere: diphenyldiazomethane,¹² KC_8 ,¹³ $L^{tBu}FeNNFeL^{tBu}$,¹³ $L^{tBu}CoN_2CPh_2$ (**1-Co**),¹⁰ $K_2[L^{tBu}CoNNCoL^{tBu}]$,¹⁴ $L^{tBu}CoCl$,^{11a} and $L^{tBu}Co$.^{11c}

NMR data were collected on an Agilent DD2 400 MHz spectrometer. Chemical shifts in 1H NMR spectra are referenced to external $SiMe_4$ using the residual protiated solvent peaks as internal standards: C_6D_5H (δ 7.16 ppm). Solution magnetic susceptibilities were determined by the Evans method.¹⁵ Elemental analyses were performed at the CENTC Elemental Analysis Facility at the University of Rochester. IR spectroscopy was run on an Alpha Platinum ATR IR spectrometer. UV-vis spectra were recorded on a Cary 50 spectrometer using Schlenk-adapted quartz cuvettes with a 1 mm path length. Cyclic voltammetry was performed under a nitrogen atmosphere using a platinum working electrode, a silver reference electrode, and a platinum wire auxiliary electrode. Tetrabutylammonium electrolyte was recrystallized three times from ethanol prior to use. Mössbauer data were recorded on a SeeCo spectrometer with alternating constant acceleration; isomer shifts are relative to iron metal at 298 K. The sample temperature was held constant in a Janis Research Company Inc. cryostat. Zero-field spectra were simulated using Lorentzian doublets with γ representing the line fitting parameter. Electron paramagnetic resonance (EPR) spectroscopy of **2-Co** was conducted using a continuous-wave Bruker EleXsys E500 EPR Spectrometer with an SHQ resonator and an Oxford Instruments ESR-9000 helium-flow cryostat. Acquisition parameters were as follows: frequency = 9.39 GHz, power = 0.020 mW, conversion time = 20.5 ms, modulation amplitude = 10 G, modulation frequency = 100 kHz, time constant = 20.5 ms, temperature = 7.6 K. EPR spectroscopy of **3-Co** was conducted using a continuous-wave Bruker EleXsys-II spectrometer. Acquisition parameters were as follows: frequency =

9.40 GHz, power = 0.0016 W, conversion time = 29 ms, modulation amplitude = 8.0 G, modulation frequency = 100 kHz, time constant = 82 ms, temperature = 12 K. EPR data were simulated using EasySpin version 5.0.5.¹⁶

CAUTION! KC_8 is a powerful reducing agent, which ignites on contact with air and moisture. Extreme care must be taken to ensure KC_8 is handled under an inert atmosphere.

CAUTION! Diazo compounds and transition metal complexes are known to be potentially explosive. Although no problems were encountered while conducting the work described herein, it is prudent to handle these compounds behind a blast shield.

Synthesis of $L^{tBu}FeN_2CPh_2$, 1-Fe. $L^{tBu}FeNNFeL^{tBu}$ (498 mg, 0.422 mmol) was dissolved in diethyl ether (40 mL). The resulting magenta solution was cooled in a liquid nitrogen cold well until it started to freeze. The solution was removed from the cold well and diphenyldiazomethane (170 mg, 0.874 mmol) was added with vigorous stirring. The solution was allowed to warm to room temperature and the color changed to yellow/brown within 30 min. Stirring was continued for another 30 min. The solution was filtered through Celite and concentrated to 15 mL under reduced pressure. Storing the solution at -40 °C led to the formation of yellow/brown crystals of **1-Fe**, suitable for single crystal X-ray diffraction (292.9 mg, 46%). Concentrating the supernatant and subsequent cooling led to further crops of **1-Fe**; however, a small amount of an unidentified impurity could be detected by 1H NMR spectroscopy. 1H NMR (400 MHz, 298 K, C_6D_6): δ 83.9 (1H; γ -H), 53.1 (4H; Ph *o*-H, Dipp *m*-H, Ph *m*-H or *i*-Pr CH), 28.5 (18H; *t*-Bu), -4.3 (4H; Ph *o*-H, Dipp *m*-H, Ph *m*-H or *i*-Pr CH), -20.1 (12H; *i*-Pr CH_3), -54.2 (4H; Ph *o*-H, Dipp *m*-H, Ph *m*-H or *i*-Pr CH), -55.7 (2H; *p*-Ar), -76.6 (12H; *i*-Pr CH_3), -90.9 (2H; *p*-Ar), -91.7 (4H; Ph *o*-H, Dipp *m*-H, Ph *m*-H or *i*-Pr CH) ppm. Solution magnetic moment (296 K, C_6D_6): $\mu_{eff} = 4.6(1) \mu_B$. UV-vis (hexanes solution): $\lambda = 310$ nm ($\epsilon = 19.4(7) \text{ mM}^{-1} \text{ cm}^{-1}$), 336 nm ($\epsilon = 22(1) \text{ mM}^{-1} \text{ cm}^{-1}$), 386 nm ($\epsilon = 13.2(6) \text{ mM}^{-1} \text{ cm}^{-1}$), 431 nm ($\epsilon = 11.3(6) \text{ mM}^{-1} \text{ cm}^{-1}$), 562 nm ($\epsilon = 0.81(6) \text{ mM}^{-1} \text{ cm}^{-1}$), 692 nm ($\epsilon = 1.0(1) \text{ mM}^{-1} \text{ cm}^{-1}$). IR (neat solid ATR, cm^{-1}): 2959(w), 2901(w), 2868(w), 1590(w), 1529(w), 1486(m), 1460(w), 1430(w), 1373(m), 1354(m), 1315(m), 1253(m), 1216(w), 1194(w), 1177(w), 1151(w), 1130(w), 1107(w), 1095(w), 1076(w), 1055(w), 1028(w), 961(w), 930(w), 901(w), 889(w), 807(w), 797(w), 778(w), 761(m), 752(m), 714(w), 690(m), 660(m), 620(w), 588(w), 528(w), 478(w), 430(w), 408(w). Elem. Anal. Calculated for $C_{48}H_{63}N_4Fe$ (%): C, 76.68; H, 8.45; N, 7.45; Found (%): C, 76.39; H, 8.49; N, 7.35. ^{57}Fe Mössbauer (80 K): $\delta = 0.58 \text{ mm s}^{-1}$; $| \Delta E_Q | = 1.81 \text{ mm s}^{-1}$.

Synthesis of $[L^{tBu}Fe(\mu-\eta^2-\eta^1-N_2CPh_2)K(OEt)_2]_2$, 2-Fe. A yellow/brown solution of **1-Fe** (97.7 mg, 0.130 mmol) in Et_2O (10 mL) was cooled in a liquid nitrogen bath until the solution began to freeze. KC_8 (21.9 mg, 0.162 mmol) was added and the resulting purple slurry was allowed to warm, with stirring, to room temperature for 1 h. The volatile components were removed under reduced pressure and the resulting purple/black solid was extracted with Et_2O (5 mL) and filtered through Celite. Volatile components were removed under reduced pressure. Crystals of **2-Fe**, suitable for single crystal X-ray diffraction, could be grown by layering concentrated Et_2O solutions of the purple solid with pentane and allowing the solvents to diffuse at room temperature, although other products cocrystallized. Further attempts to purify **2-Fe** were unsuccessful and therefore spectroscopic characterization was not possible. Crude 1H NMR and IR spectra are included in the Supporting Information. The crude yield was 22.5 mg (20%).

Synthesis of $[L^{tBu}Co(\mu-\eta^2-\eta^1-N_2CPh_2)K(OEt)_2]_2$, 2-Co, Method A. A brown/green solution of $L^{tBu}CoN_2CPh_2$, **1-Co** (89.2 mg, 0.118 mmol), in Et_2O (8 mL) was cooled for 5 min in a dry ice/acetone cold bath. KC_8 (17.6 mg, 0.130 mmol) was added and the resulting purple slurry was allowed to warm, with stirring, to room temperature for 1 h. The volatile components were removed under vacuum and the resulting purple/black solid was extracted with Et_2O (10 mL) and filtered through Celite. The filter cake was washed with Et_2O (25 mL) until the filtrate was colorless. Volatile components were removed under reduced pressure and the resulting purple solid contained **2-Co** and <10% impurities as judged by 1H NMR spectroscopy (96.3 mg,

crude yield 74%). Layering a concentrated solution of crude product in Et₂O (10 mL) with pentane (4 mL) and allowing solvents to diffuse at -40 °C for 5 d afforded 16.4 mg of dark purple crystals of pure **2-Co**. Concentrating the mother liquor to 4 mL and storing at -40 °C for 1 week afforded an additional 18.1 mg (combined yield of 34.5 mg, 34%). ¹H NMR (400 MHz, 298 K, C₆D₆) δ 15.2, 11.8, 9.9, 8.6, 5.7, 2.5, 1.8, 1.4, -1.9, -8.7 ppm. Due to the extent of paramagnetic broadening of the NMR spectrum of **2-Co**, reliable peak integrations could not be obtained. Solution magnetic moment (296 K, THF-*d*₈): μ_{eff} = 1.7(1) μ_B. UV-vis (Et₂O solution): λ = 335 nm (ε = 109(6) mM⁻¹ cm⁻¹), 392 nm (shoulder; ε = 53(2) mM⁻¹ cm⁻¹), 451 nm (shoulder; ε = 38(3) mM⁻¹ cm⁻¹), 563 nm (ε = 49(5) mM⁻¹ cm⁻¹). IR (neat solid ATR, cm⁻¹): 2953(m), 2927(w), 2903(w), 2865(s), 1580(m), 1530(w), 1484(m), 1462(w), 1432(m), 1383(s), 1360(s), 1339(s), 1317(s), 1292(s), 1247(m), 1216(m), 1188(m), 1173(m), 1160(m), 1098(m), 1055(w), 1027(w), 992(w), 964(w), 946(w), 935(w), 922(w), 897(w), 876(w), 847(w), 807(w), 781(m), 746(s), 706(m), 693(m), 680(m), 633(w), 575(w), 552(w), 492(w), 451(w), 422(w). Elem. Anal. Calculated for C₁₀₄H₁₄₆N₈O₂K₂Co₂ (%): C, 71.94; H, 8.48; N, 6.45; Found (%): C, 71.98; H, 8.47; N, 5.96.

Synthesis of [L^{tbu}Co(η²-N₂CPh₂)₂·K(OEt₂)₂], **2-Co, Method B.** Diphenyldiazomethane (62 mg, 0.32 mmol) was added to a black solution of K₂[L^{tbu}CoNNCoL^{tbu}] (249 mg, 0.151 mmol) in THF (10 mL). The resulting deep purple solution was stirred for 14 h. The volatile components were removed under reduced pressure and the resulting purple/black solid was extracted with Et₂O (35 mL). The deep purple solution was concentrated to 15 mL under reduced pressure and crystals of **2-Co** started to form. These crystals were isolated (54 mg) and the supernatant was cooled to -40 °C. This yielded a further crop of **2-Co** (85 mg; total yield = 53%).

Synthesis of [L^{tbu}Co(η²-N₂CPh₂)₂·K(OEt₂)₂], **2-Co, Method C.** A red/brown solution of L^{tbu}CoCl (567 mg, 0.951 mmol) in Et₂O (30 mL) was cooled in a liquid nitrogen bath until the solution began to freeze. KC₈ (142 mg, 1.05 mmol) was added and the resulting slurry was allowed to warm, with stirring, for 17 h. The brown slurry was again cooled in a liquid nitrogen bath until it began to freeze. Diphenyldiazomethane (203 mg, 1.05 mmol) was added and the slurry was stirred as the solution warmed to room temperature over the course of 1 h. No color change was observed, and the slurry was cooled a final time in a liquid nitrogen bath until it began to freeze. KC₈ (142 mg, 1.05 mmol) was added and the slurry instantly changed to a purple color with formation of a black solid. The slurry was warmed to room temperature, with stirring, over the course of 3.5 h. Volatile components were removed under vacuum. The resulting dark solid was extracted with Et₂O (120 mL) and filtered to yield an intensely colored purple solution. Volatile components were removed under vacuum and the resulting purple solid was washed with pentane (30 mL). This purple solid was pure as judged by ¹H NMR spectroscopy (500 mg, yield = 61%).

Synthesis of [L^{tbu}CoN₂CPh₂]₂[K(18-c-6)], **3-Co.** To a dark purple solution of **2-Co** (201 mg, 0.116 mmol) in THF (10 mL) was added 18-crown-6 (18-c-6; 66.5 mg, 0.252 mmol). The resulting purple solution was stirred for 1.25 h. The volatile components were removed under reduced pressure and the resulting waxy purple solid was washed with pentane (5 mL). A purple powder remained and excess pentane was removed under reduced pressure. This solid was extracted with toluene (4 mL) and filtered through Celite. Layering the toluene solution with pentane and allowing the solvents to diffuse at room temperature resulted in the formation of crystals of **3-Co**, suitable for single crystal X-ray diffraction (118 mg, yield = 47%). ¹H NMR (400 MHz, 298 K, C₆D₆) δ 16.3, 11.1, 5.6, 5.1, 2.5, 1.9, 1.4, 0.9, -0.5 ppm. Due to the extent of paramagnetic broadening of the NMR spectrum of **3-Co**, reliable peak integrations could not be obtained. Solution magnetic moment (296 K, C₆D₆): μ_{eff} = 1.5(1) μ_B. UV-vis (hexanes): λ = 333 nm (ε = 23.7(2) mM⁻¹ cm⁻¹), 401 nm (shoulder; ε = 14.2(2) mM⁻¹ cm⁻¹), 452 nm (shoulder; ε = 10.92(6) mM⁻¹ cm⁻¹), 569 nm (ε = 10.72(9) mM⁻¹ cm⁻¹), 614 nm (shoulder; ε = 7.13(6) mM⁻¹ cm⁻¹). IR (neat solid ATR, cm⁻¹): 2952(m), 2895(m), 2858(m), 1580(w), 1485(w), 1471(w), 1429(m), 1376(m), 1351(m), 1316(m), 1285(w), 1244(m), 1219(w), 1182(w), 1149(w), 1131(w), 1101(s),

1054(w), 1029(w), 991(w), 961(m), 927(w), 892(w), 836(w), 795(w), 758(w), 724(w), 693(w), 673(w), 579(w), 557(w), 541(w), 530(w), 506(w), 489(w), 449(w), 419(w). Elem. Anal. Calculated for C₄₉H₆₆N₄Co·K(C₁₂H₂₄O₆) (%): C, 68.25; H, 8.45; N, 5.22; Found: C, 68.49; H, 8.24; N, 5.11.

Synthesis of L^{tbu}CoPF₆, **4-Co-PF₆.** Under an argon atmosphere, L^{tbu}Co (148 mg, 0.264 mmol) was dissolved in diethyl ether (10 mL). The resulting brown-yellow solution was added to a stirring slurry of silver hexafluorophosphate (82.7 mg, 0.327 mmol) in diethyl ether (4 mL), giving a green reaction with dark precipitate. The heterogeneous reaction was allowed to stir for 6 h and then passed through Celite to remove a dark gray precipitate. Volatile components were removed under vacuum to afford a yellow-green powder, which was extracted into pentane (6 mL) and filtered through Celite. The resulting green filtrate was concentrated to 5 mL under reduced pressure and stored at -40 °C for 3 d to afford dark green crystals (54.4 mg) that contained minor impurities as judged by proton NMR spectroscopy. Analytically pure **4-Co-PF₆** was obtained by dissolving the green crystals in pentane (5 mL), concentrating the solution to 3 mL under reduced pressure, filtering through Celite, and storing the green filtrate at -40 °C for 5 d to give dark green rectangular crystals suitable for X-ray diffraction (21.2 mg, 11%). ¹H NMR (400 MHz, 298 K, C₆D₆) δ 34.2 (4H, *i*-Pr CH or aryl *m*-H), 27.0 (18H, *t*-Bu), -7.7 (12H, *i*-Pr CH₃), -44.2 (1H, γ -H), -50.8 (12H, *i*-Pr CH₃), -66.0 (4H, *i*-Pr CH or aryl *m*-H), -73.4 (2H, aryl *p*-H) ppm. Solution magnetic moment (298 K, C₆D₆): μ_{eff} = 4.6(1). UV-vis (toluene): λ = 340 nm (ε = 23.3 mM⁻¹ cm⁻¹), 430 nm (shoulder; ε = 0.704 mM⁻¹ cm⁻¹), 510 nm (shoulder; ε = 0.249 mM⁻¹ cm⁻¹), 620 nm (ε = 0.209 mM⁻¹ cm⁻¹). IR (solid ATR, cm⁻¹): 3061(w), 2962(m), 2931(m), 2871(w), 1538(w), 1505(m), 1492(m), 1464(m), 1431(m), 1403(w), 1377(m), 1347(s), 1315(s), 1281(m), 1253(w), 1219(m), 1194(m), 1155(w), 1135(w), 1098(m), 1055(w), 1029(m), 915(s), 856(vs), 799(m), 781(m), 753(m), 724(s), 679(w), 546(s), 483(m), 434(m), 412(w). Elem. Anal. Calculated for C₃₅H₅₃CoF₆N₂P (%): C, 59.57; H, 7.57; N, 3.97 Found (%): C, 59.73; H, 7.46; N, 3.89.

Computational Studies. Density Functional Theory (DFT) calculations were performed using the Gaussian 09 suite of programs.¹⁷ Natural Bond Order (NBO) studies were performed using NBO 6.0 through the Gaussian 09 interface.¹⁸ These calculations were performed at the Yale University Faculty of Arts and Sciences High Performance Computing Center. Representative input files are included in the [Supporting Information](#).

Due to the size of 1–3 and the requirements of the NBO 6.0 program, three basis sets were used at different stages of the computational studies. B1 employed the SDD basis set with an effective core potential for the transition metal atom, the 6-31++G(d,p) double- ζ basis set for the nitrogen atoms and the central carbon atom on the diazoalkane moiety and the 6-31G double- ζ basis set was used for all remaining atoms. B2 employed the SDD basis set with an effective core potential for the transition metal atom and the 6-311++G(d,p) triple- ζ basis set for all remaining atoms. B3 employed the SDD basis set with an effective core potential for the transition metal atom and the 6-311G(d,p) triple- ζ basis set for all remaining atoms. For **2-Co**, potassium was treated with the SDD basis set with an effective core potential for B1–B3 (for further clarification see [Supporting Information, Figure S24](#)).

Geometry optimizations started from the atomic coordinates of the respective crystal structures. Spin states for optimizations of **1-Fe**, **2-Co** and **3-Co** were selected based on those experimentally determined. The full molecule of **1-Fe** (neutral quartet) was optimized to give a geometry **1-Fe-DFT**. In order to save computational resources only the monomeric unit of **2-Co** (neutral doublet) and the anionic component of **3-Co** (anionic doublet), without the corresponding potassium 18-c-6 cation, were optimized, yielding the corresponding geometries **2-Co-DFT** and **3-Co-DFT**.

As with our previous study on **1-Co**,¹⁰ we found that optimization with M06L/B1 consistently gave geometries that were in better agreement with the experimentally determined geometries than either PBE0/B1 or ω B97xD/B1 (based on comparison of the metrical parameters, as well as calculating the RMS error for the distance

between each atom in the crystal structure with the corresponding atom in the calculated geometry when the two structures were overlaid). For all optimizations, the D3 dispersion scheme, developed by Grimme and co-workers,¹⁹ was applied for the M06L and PBE0 functionals, while the inbuilt dispersion scheme was used for the ω B97xD functional.²⁰ Furthermore, a pruned 99,590 point grid was used for the integration (ultrafine) and the SCF convergence criteria were increased to 10^{-9} . Final geometries of **1-Fe-DFT**, **2-Co-DFT**, and **3-Co-DFT** were determined by increasing the optimization convergence criteria to very tight and reoptimizing with M06L/B1 (coordinates for the optimized geometries are included in the Supporting Information).

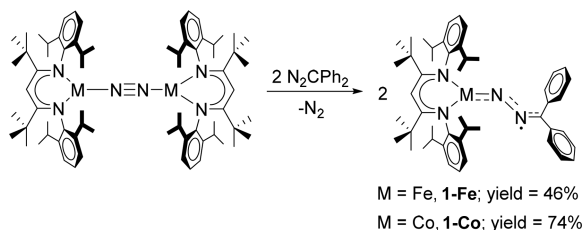
The wave functions of **1-Fe-DFT**, **2-Co-DFT**, and **3-Co-DFT** were stable (M06L/B1) with respect to relaxed constraints using the inbuilt function of Gaussian 09. The geometries were also determined to be minima on the potential energy surfaces as no imaginary frequencies were calculated for **1-Fe-DFT**, **2-Co-DFT**, or **3-Co-DFT**.

The electronic structures of **1-Fe-DFT**, **2-Co-DFT**, and **3-Co-DFT** were calculated using the hybrid functional M06/B2, though M06L gave qualitatively similar results.²¹ The α - and β -spin orbitals were maximally aligned using the guess = BiOrth option in Gaussian 09. Subsequent electronic analysis of **1-Fe-DFT**, **2-Co-DFT**, and **3-Co-DFT** was performed using NBO 6.0 and M06/B3 on unrestricted wave functions.

RESULTS

Treating the iron(I) dinitrogen complex $L^{tBu}FeNNFeL^{tBu11b}$ with diphenyldiazomethane led to yellow-brown crystals of $L^{tBu}FeN_2CPh_2$ (**1-Fe**) in moderate yield (46%; Scheme 1). The

Scheme 1. Synthesis of $L^{tBu}FeN_2CPh_2$, **1-Fe**, and $L^{tBu}CoN_2CPh_2$, **1-Co**.¹⁰



molecular structure of **1-Fe** is very similar to that of **1-Co**, and features a doubly bent diazoalkane moiety terminally bound to a trigonal-planar iron center ($\Sigma_{Fe} = 360.0^\circ$, Figure 2). As in **1-Co**, there is evidence for multiple bond character between the transition metal and the coordinated diazoalkane, because the Fe1–N14 bond length in **1-Fe** (1.752(1) Å) is shorter than the Fe–N single bond in the three-coordinate iron(II) amido complexes $L^{tBu}FeN(H)R$ (1.787–1.902 Å; R = Ph, Dipp, *t*Bu, *p*-tolyl, mesityl).²² However, the distance is longer than the Fe=N double bond in the three-coordinate iron imido complexes $L^{Me}Fe=NAd$ and $L^{Ph}Fe=NAd$ (1.670 and 1.700 Å, respectively; $L^{Me} = [(\text{Dipp})\text{NC}(\text{Me})_2\text{CH}]^-$, $L^{Ph} = [(\text{2,4,6-Ph}_3\text{C}_6\text{H}_2)\text{NC}(\text{Me})_2\text{CH}]^-$).²³ (For a summary of selected bond lengths and angles, see Table 1.) Furthermore, the Fe1–N14 bond in **1-Fe** is shorter than the Fe–N_{diazo} bond in the four-coordinate iron diazoalkane complex $[\text{tpeFeN}_2\text{CPh}_2][\text{Li}(\text{THF})]$ (1.781(9) Å; tpe = tris(5-mesitylpyrrolyl)ethane), the only other reported example of an iron diazoalkane complex with significant diazoalkane radical anion character.^{9b}

The previously reported iron(I) dinitrogen complexes $L^{tBu}FeNNFeL^{tBu}$ and $L^{Me}FeNNFeL^{Me}$ feature three-coordinate iron centers coordinated to three N-donor ligands, as in **1-Fe**.^{11b,13} Significantly, detailed spectroscopic and computational

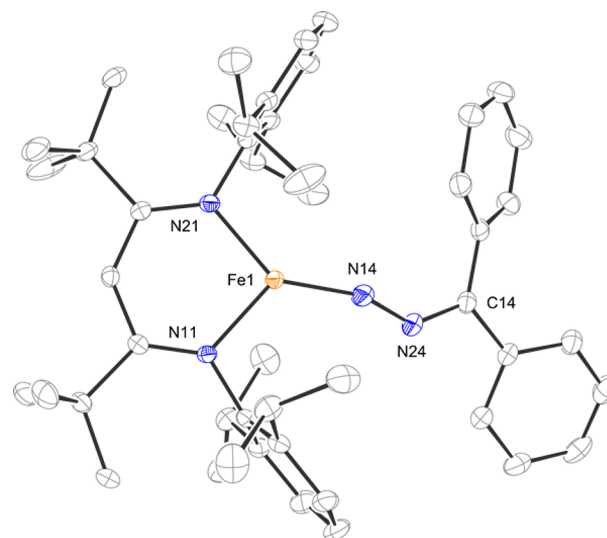


Figure 2. Molecular structure of $L^{tBu}FeN_2CPh_2$, **1-Fe**. Thermal ellipsoids displayed at the 50% probability level and hydrogen atoms are omitted for clarity. For selected bond lengths and angles, see Table 1.

studies suggest that charge transfer occurs from the formally iron(I) centers to the bound N_2 ligand, resulting in two iron(II) centers, antiferromagnetically coupled to triplet N_2^{2-} .²⁴ The Fe–N bonds in $L^{tBu}FeNNFeL^{tBu}$ and $L^{Me}FeNNFeL^{Me}$ (Fe–N₂: 1.746–1.775 Å; Fe–N_{nacnac}: 1.945–1.984 Å) have similar lengths as those in **1-Fe** (Fe1–N14:1.752(1) Å; Fe1–N11:1.952(1) Å; Fe1–N21:1.942(1) Å). Finally, the Fe–N_{nacnac} bond lengths in **1-Fe** are shorter than the range of previously reported Fe–N_{nacnac} bond lengths in the three-coordinate iron(II) amido complexes $L^{tBu}FeNHR$ (1.961–2.018 Å; R = Ph, Dipp, *t*Bu, *p*-tolyl, mesityl),²² further supporting diazoalkane reduction by a single electron to give a Fe^{2+} -diazoalkane[−] structure.

Further corroborating evidence for the presence of a diazoalkane radical anion comes from the doubly bent geometry of the Fe–N–N–C unit in **1-Fe**. As in **1-Co**,¹⁰ the M–N–N and N–N–C angles (Fe1–N14–N24 154.3(1)°, N14–N24–C14 133.2(1)°) do not tend to 120° or 180°, but are intermediate between the two extremes usually observed for transition metal diazoalkane complexes. Compound **1-Fe** also features an N14=N24 double bond (1.243(2) Å) and a long N24=C14 double bond (1.319(2) Å),²⁵ which are again in good agreement with those in **1-Co**. This geometry remains rare in the literature, as there are only three other complexes, apart from **1-Co** and $[\text{tpeFeN}_2\text{CPh}_2][\text{Li}(\text{THF})]$, that feature similar bond lengths and angles and the diazoalkane geometry is not constrained as part of a chelate.^{24,26}

Spectroscopic characterization of **1-Fe** contains many parallels with that for **1-Co**.¹⁰ Compound **1-Fe** displays averaged C_{2v} symmetry in solution, as evidenced by the 10-line pattern in its ¹H NMR spectrum. No IR stretching modes could be definitively assigned to the N–N stretching vibration, presumably because these are obscured by aromatic and C–N stretching bands from the supporting ligand. The solution magnetic moment (4.6(1) μ_B) was larger than the spin-only value for an $S = 3/2$ ground state (3.87 μ_B), which is likely to arise from orbital contributions to the magnetic moment as observed in other diketiminate-supported iron(I) and iron(II) complexes.²⁴ However, these magnetic data are consistent with

Table 1. Selected Bond Lengths and Angles for the Compounds That Are Reported in This Article^a

	1-Fe/1-Fe-DFT	1-Co ^b /1-Co-DFT ^b	2-Fe	2-Co/2-Co-DFT	3-Co/3-Co-DFT
M–N11 (Å)	1.952(1)/1.980	1.902(2)/1.949	1.957(1)	1.896(3)/1.904	1.887(3)/1.937
N–N21 (Å)	1.942(1)/1.953	1.916(2)/1.910	1.936(1)	1.910(4)/1.938	1.885(3)/1.920
M–N14 (Å)	1.752(1)/1.750	1.719(2)/1.724	1.839(2)	1.804(4)/1.816	1.703(3)/1.742
M–N24 (Å)			1.937(2)	1.929(4)/1.912	
N14–N24 (Å)	1.243(2)/1.238	1.216(2)/1.218	1.288(2)	1.271(5)/1.290	1.264(4)/1.235
N24–C14 (Å)	1.319(2)/1.323	1.322(3)/1.317	1.357(2)	1.386(6)/1.340	1.341(5)/1.342
M–N14–N24 (deg)	154.3(1)/154.9	159.4(2)/159.6			155.3(3)/154.0
N14–N24–C14 (deg)	133.2(1)/133.6	134.2(2)/139.2	125.2(2)	125.0(4)/129.4	131.4(4)/133.2

^aThe crystallographically determined geometrical parameter appears first, followed by the one calculated by DFT. ^bThis compound and the corresponding geometry-optimized structure were previously reported.¹⁰

either a high-spin iron(I) diazoalkane adduct or high-spin iron(II) antiferromagnetically coupled to a diazoalkane radical anion, because both have $S = 3/2$ ground states. Multiple attempts to collect EPR data on **1-Fe** revealed no signals, both in a toluene glass and as solid. There are precedents for large zero-field splitting in $S = 3/2$ cobalt(II) complexes, which can render them EPR-silent at X-band frequencies.²⁷

An advantage of the iron complex **1-Fe** over the earlier reported cobalt complex **1-Co** is that ⁵⁷Fe Mössbauer spectroscopy can provide further insight into the electronic environment of the iron center. The quadrupole doublet of **1-Fe** ($\delta = 0.58 \text{ mm s}^{-1}$, $|\Delta E_Q| = 1.81 \text{ mm s}^{-1}$; see Figure S6) is quite similar to that for the iron dinitrogen complex $L^{\text{Me}}\text{FeNNFeL}^{\text{Me}}$ ($\delta = 0.58(1) \text{ mm s}^{-1}$, $|\Delta E_Q| = 1.41(1) \text{ mm s}^{-1}$).²⁴ As discussed above, the proposed iron environment in **1-Fe** is very similar to that in $L^{\text{Me}}\text{FeNNFeL}^{\text{Me}}$, where detailed computational and Mössbauer studies supported an iron(II)-ligand radical formulation. Based on this spectroscopic characterization of **1-Fe**, we therefore favor an assignment of high-spin iron(II) antiferromagnetically coupled to diphenyldiazomethane radical anion and this is supported by computational studies (see below).

In order to further explore electronic effects on diazoalkane ligands, we performed cyclic voltammetry (ca. 1 mM solutions in THF, Figure 3) on complexes **1-Fe** and **1-Co**. The cyclic voltammogram of each compound features a reversible single-

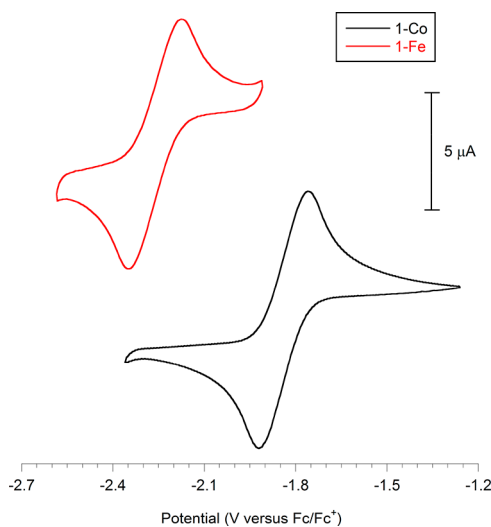


Figure 3. Cyclic voltammograms of 1 mM **1-Co** and 1 mM **1-Fe** in THF using 0.1 M tetrabutylammonium hexafluorophosphate electrolyte and platinum working electrode. Scan rate: 500 mV/s.

electron reduction event (**1-Fe**: -2.26 V versus Fc^+/Fc , **1-Co**: -1.84 V versus Fc^+/Fc). An irreversible single-electron oxidation event is also evident in the voltammogram of each compound, which we assign to loss of diazoalkane upon oxidation of $L^{\text{tBu}}\text{M}^2+\text{N}_2\text{CPh}_2^{\cdot-}$ (**1-Fe**: -0.75 V ; **1-Co**: -0.28 V ; see below for chemical oxidation of **1-Fe** and **1-Co**; see Supporting Information, Figures S5 and S1 for full voltammograms).

In order to understand the nature of the reduced product, compounds **1-Fe** and **1-Co** were each treated with 1 equiv of KC_8 in diethyl ether. In each case, this resulted in an intensely colored purple solution. Following workup, the reduced species $[\text{L}^{\text{tBu}}\text{Fe}(\mu-\eta^2:\eta^1-\text{N}_2\text{CPh}_2)\text{K}(\text{OEt}_2)]_2$, **2-Fe**, and $[\text{L}^{\text{tBu}}\text{Co}(\mu-\eta^2:\eta^1-\text{N}_2\text{CPh}_2)\text{K}(\text{OEt}_2)]_2$, **2-Co**, were isolated (20% and 74%, respectively; Scheme 2). Crystals of each compound were grown from concentrated diethyl ether solutions when layered with pentane, although other unidentified products cocrystallized with **2-Fe**. These crystals were suitable for single crystal X-ray diffraction studies using either Mo $K\alpha$ radiation (**2-Co**) or synchrotron radiation ($\lambda = 0.7749 \text{ \AA}$; **2-Fe**). Compounds **2-Fe** and **2-Co** are nearly isostructural, and reveal that the binding mode of the diazoalkane changed upon reduction from terminal N-bound to η^2 -N,N' (for **2-Co** see Figure 4, for **2-Fe** see Supporting Information, Figure S7).

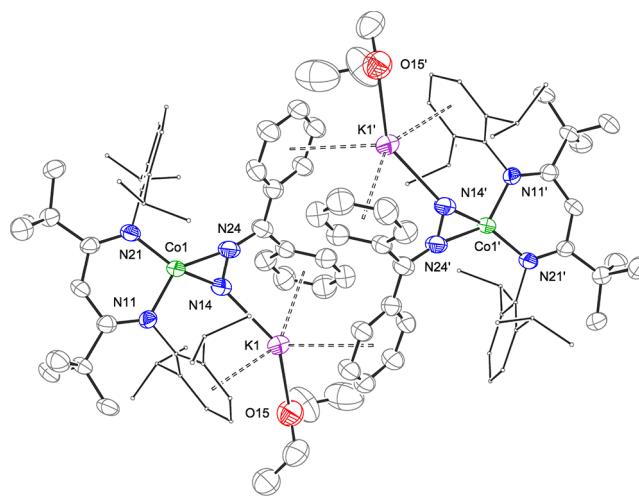
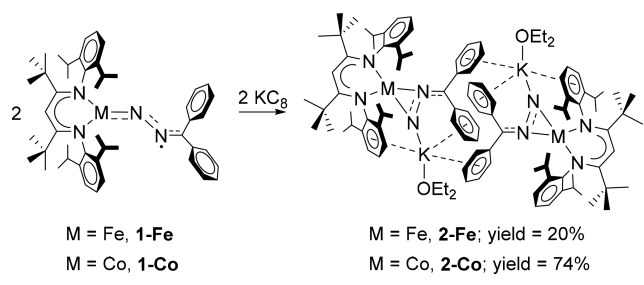


Figure 4. Molecular structure of $[\text{L}^{\text{tBu}}\text{Co}(\mu-\eta^2:\eta^1-\text{N}_2\text{CPh}_2)\text{K}(\text{OEt}_2)]_2$, **2-Co**. Thermal ellipsoids are displayed at the 50% probability level. Hydrogen atoms are omitted and Dipp groups are displayed in wireframe format for clarity. For selected bond lengths and angles, see Table 1.

Scheme 2. Synthesis of $[L^{tBu}Fe(\mu-\eta^2:\eta^1-N_2CPh_2)K(OEt_2)]_2$, 2-Fe, and $[L^{tBu}Co(\mu-\eta^2:\eta^1-N_2CPh_2)K(OEt_2)]_2$, 2-Co



The *formally* iron(0) and cobalt(0) centers in 2-Fe and 2-Co, respectively, adopt distorted square planar geometries to accommodate the change in ligand binding mode ($\Sigma_{Fe} = 361.0^\circ$; $\Sigma_{Co} = 361.1^\circ$). There is little change in the M-N_{Nacnac} bond lengths upon reduction from 1-Fe to 2-Fe or 1-Co to 2-Co (Table 1). However, due to the change in coordination number, it is difficult to draw definitive conclusions with respect to the oxidation state of the metal centers in 2-Fe and 2-Co based on crystallographic evidence alone.

Crystallography does, however, help to evaluate the oxidation level of the diazoalkane moieties in 2-Fe and 2-Co, and the oxidation states of the metal centers can be inferred from these. In the molecular structures of the reduced compounds 2-Fe and 2-Co, the diazoalkane moieties are bent at N14–N24–C14. Lengthening of the N24–C14 bonds to short single bonds²⁵ in 2-Fe (1.357(2) Å) and 2-Co (1.386(6) Å) suggests further reduction of the diazoalkane ligand by population of ligand based π^* antibonding orbitals. The N14–N24 bonds in 2-Fe and 2-Co remain consistent with N=N double bonds (1.288(2) Å and 1.271(5) Å, respectively).²⁵ The shorter M–N14 bonds (Fe1–N14 1.839(2) Å and Co1–N14 1.804(4) Å) relative to the M–N24 bonds (Fe1–N24 1.937(2) Å and Co1–N24 1.929(4) Å) are consistent with an assignment of the former as single bonds, and the latter as dative interactions between an N-centered lone-pair and the transition metal center. These metrical parameters are consistent with previously reported side-on bound diazoalkane complexes which also feature N–N double bonds (1.236–1.280 Å), C–N single bonds (1.331–1.367 Å), one M–N covalent bond and one M–N dative bond.^{4b,5d,28} This is usually assigned as a 2e[−] reduction of the diazoalkane ligand,^{1d} and the only prior example of an η^2 -diazoalkane ligand assigned as a radical anion featured a longer N–N bond (1.338(5) Å).^{9a}

The potassium ions in 2-Fe and 2-Co are bound to N14 of one diazomethane and coordinated diethyl ether, and also have three η^3 -aryl interactions (one to L^{tBu} and one to each diphenyldiazomethane). The K1–N14 bond length (2.760(4) Å) is shorter than the K–N dative interaction in K(18-crown-6)N₃·H₂O (2.896 Å)²⁹ but longer than the sum of the covalent single bond radii (2.67 Å).²⁵ As 2-Fe could not be isolated as a pure solid, and the metrical parameters from the single crystal X-ray diffraction studies are similar for both species, further discussion of characterization data will be limited to 2-Co.

Compound 2-Co has an $S = 1/2$ ground state, as indicated by the solution magnetic moment (1.7(1) μ_B). The EPR spectrum of 2-Co in a 1:1 toluene/THF glass (Figure 5) is consistent with this spin state. However, despite the purity as judged by microanalysis, the experimental EPR spectrum of 2-Co could only be adequately simulated using a combination of two signals. The first species (notated Component A) is a

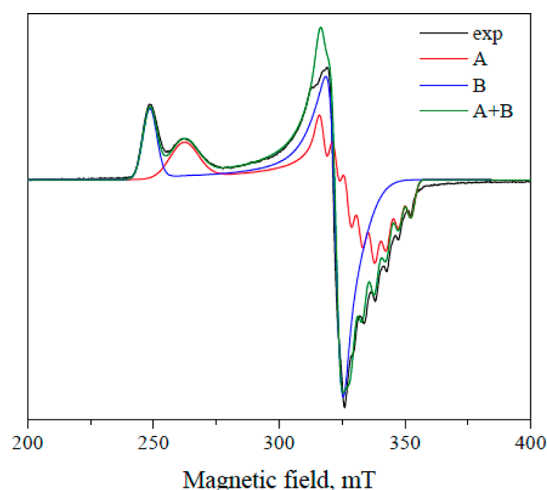


Figure 5. X-band EPR spectrum of 2-Co in toluene/THF at 7.6 K. The experimental spectrum (black) was simulated using a linear combination (green) of 50% component A (red) and 50% component B (blue) as described in the text.

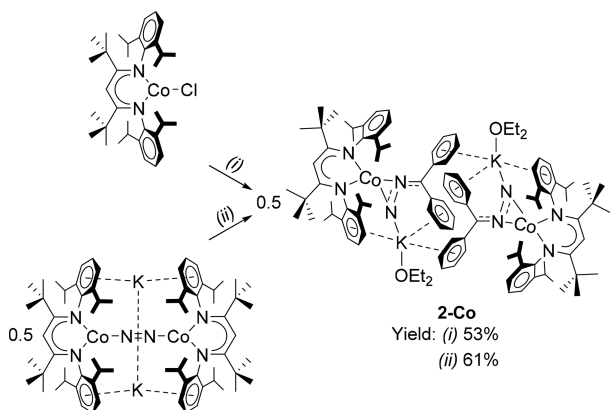
nearly axial $S = 1/2$ species with g -values of 2.555, 2.015, and 2.001, and has clearly defined ⁵⁹Co hyperfine features with $A = 17.0, 46.2,$ and 137 MHz. Anisotropic line broadening of Component A was simulated using H-strain values of 462, 186, and 99.3 MHz. Component B is a nearly axial $S = 1/2$ species with g -values of 2.696, 2.044, and 2.073, and does not have defined ⁵⁹Co features. Anisotropic line broadening of Component B was simulated using H-strain values of 242, 511, and 143 MHz. The most precise fit of the experimental data was a linear combination of 50% of Component A and 50% of Component B. The appearance of two components could be due to an equilibrium involving a change in the diazoalkane coordination mode; it is unlikely that it is a solvent-based equilibrium, because monitoring 2-Co by variable-temperature ¹H NMR between -80 and 20 °C showed no changes in solution speciation (Supporting Information, Figure S10b). Additionally, the EPR spectrum of 2-Co measured in neat toluene shows only a slight change in the ratio of Component A to Component B from 50:50 in toluene/THF to 61:39 (Supporting Information, Figure S14). The ¹H NMR spectrum of 2-Co has few peaks because of severe paramagnetic broadening, as is typical for compounds with a $S = 1/2$ ground state; however, it contains one diagnostic resonance (δ 15.2 ppm) that can be used for identification. Based on the spin state and structural parameters determined by X-ray crystallography, 2-Co could be assigned as having cobalt(I) antiferromagnetically coupled to a diazoalkane radical anion, or a cobalt(II) hydrazonido complex. Computational studies (see below) favor the latter description.

No N–N stretching modes could be definitively assigned in the IR spectrum of 2-Co. 2-Co is stable in solution for 24 h at elevated temperatures (80 °C), as judged by ¹H NMR spectroscopy. Treating 2-Co with Lewis acids (Sm(OTf)₃, La(OTf)₃, BPh₃, B(C₆F₅)₃) either led to no reaction or a mixture of 1-Co and other (unidentified) products. Attempts to reduce 2-Co with a further molar equivalent of KC₈ did not result in any reaction, as judged by ¹H NMR spectroscopy.

Compound 2-Co can also be synthesized from the *formally* cobalt(0) dinitrogen complex K₂[L^{tBu}CoN₂CoL^{tBu}].¹⁴ Treating the cobalt(0) synthon with two molar equivalents of diphenyldiazomethane led directly to 2-Co, which could be

isolated in moderate yield (53%; Scheme 3). Furthermore, this compound could be synthesized in a “one-pot” procedure from the cobalt(II) halide complex $L^{tBu}CoCl$ using two molar equivalents of KC_8 (which forms the dinitrogen complex in situ) and subsequently a single molar equivalent of N_2CPh_2 , in an improved yield (61%; Scheme 3).

Scheme 3. Alternative syntheses of $[L^{tBu}Co(\mu-\eta^2:\eta^1-N_2CPh_2)K(OEt_2)]_2$, **2-Co**^a



^aReaction conditions: (i) 2 KC_8 , 1 N_2CPh_2 , Et_2O ; (ii) 1 N_2CPh_2 , THF.

Given the coordination of the terminal diazoalkane N atom to potassium, we were interested to learn whether the potassium ion induced the side-on coordination mode in **2-Co**. We therefore added 18-crown-6 (18-c-6) to a purple solution of **2-Co** in THF, which gave a 47% yield of the cation–anion pair $[L^{tBu}CoN_2CPh_2][K(18-c-6)]$, **3-Co** (Scheme 4). The molecular structure shows that the diazoalkane ligand reverts to a terminal binding mode (Figure 6) after potassium

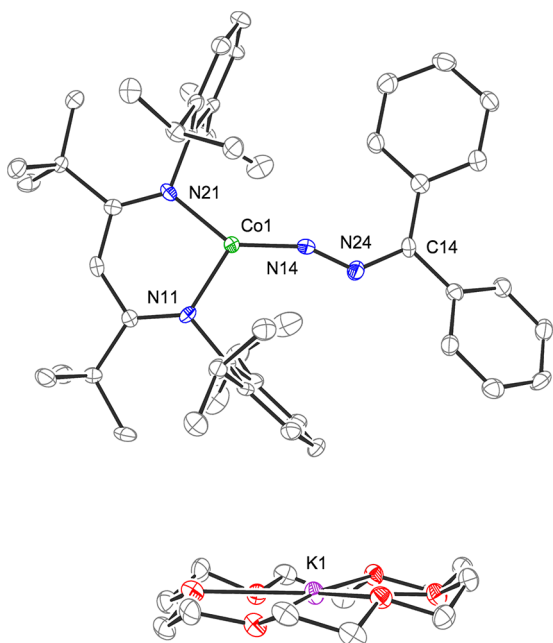
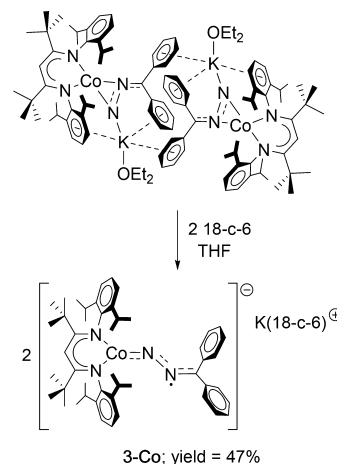


Figure 6. Molecular structure of $[L^{tBu}CoN_2CPh_2][K(18-c-6)]$, **3-Co**. Thermal ellipsoids are displayed at the 50% probability level. Hydrogen atoms are omitted for clarity. For selected bond lengths and angles, see Table 1.

extrusion. Relative to **2-Co** in which coordination of the potassium cation is observed, the structural change in **3-Co** to terminal diazoalkane binding is significant, as it demonstrates how a Lewis acid can alter the geometry of a diazoalkane complex.

Scheme 4. Synthesis of $[L^{tBu}CoN_2CPh_2][K(18-c-6)]$, **3-Co**



Although there is no *formal* oxidation state change upon potassium sequestration from **2-Co** to **3-Co**, the anionic component of **3-Co** has a structure that is reminiscent of **1-Fe** and **1-Co**. The Co1–N11/N21 bond lengths (1.887(3) Å and 1.885(3) Å, respectively) remain similar to those in **1-Co** and **2-Co** (Table 1). Surprisingly, and Co1–N14 bond length is slightly shorter in **3-Co** than **1-Co** (1.703(3) Å and 1.719(2) Å, respectively), despite a *decrease* in formal oxidation state. However, the elongated N14–N24 (1.264(4) Å) and N24–C14 (1.341(5) Å) bonds, relative to those in **1-Co**, suggest an increase in charge buildup on the diazoalkane. Despite this increase in reduction of the diazoalkane, the intermediate Co1–N14–N24 (155.3(3)°) and N14–N24–C14 (131.4(4)°) angles, and shorter N24–C14 bond (1.341(5) Å) relative to the hydrazonido ligand in **2-Co** (1.386(6) Å), suggest that the diazoalkane in **3-Co** is best described as a radical anion.

The EPR spectrum of **3-Co** is consistent with a nearly axial $S = 1/2$ species, with g -values of 2.545, 2.095, and 2.006 and ^{59}Co hyperfine features with $A = 100$, 10.0, and 137 MHz (Figure 7). The solution magnetic moment is also consistent with this spin state (1.5(1) μ_B). As with **2-Co**, the 1H NMR spectrum of **3-Co** is paramagnetically broadened. However, there is a shift of the diagnostic resonance of **2-Co** (δ 15.2 ppm) upon sequestration of the potassium cation with crown ether to form **3-Co** (δ 16.3 ppm). As with the previously discussed compounds, no N–N stretching mode was identified in the IR spectrum of **3-Co**. This spectroscopic characterization is consistent with high-spin cobalt(1) antiferromagnetically coupled to a diazoalkane radical anion with an overall $S = 1/2$ ground state.

Although stable in solution at elevated temperature (60 °C) for 36 h, **3-Co** decomposes within 12 h at 80 °C as determined by proton NMR spectroscopy, as compared to **2-Co** which is stable for more than a day at 80 °C. Thus, the presence of the alkali metal within the structure of **2-Co** is stabilizing. As with **2-Co**, the addition of Lewis acids to **3-Co** gave either no reaction or product mixtures containing **1-Co**.

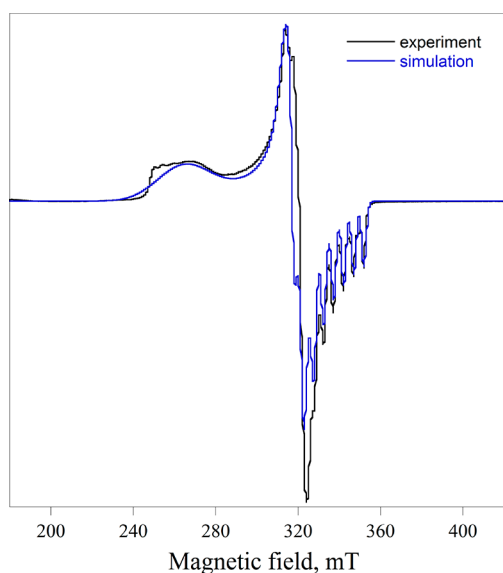


Figure 7. X-band EPR spectrum of **3-Co** in toluene at 12 K. The experimental spectrum (black) was simulated using H-Strain values of 900, 196, and 60.0 MHz.

Consistent with the irreversible oxidation peak that was evident in the cyclic voltammograms of **1-Fe** and **1-Co**, attempts to oxidize each compound with AgOTf or AgPF₆ did not lead to diazoalkane containing complexes. Oxidation of **1-Fe** with AgOTf instead afforded the previously reported compound L^{tBu}FeOTf,³⁰ in addition to benzophenone azine as identified by ¹H NMR spectroscopy and GC-MS. No other organic products (such as tetraphenylethylene) were identified. Likewise, oxidation of **1-Co** with AgPF₆ formed a new paramagnetic product and benzophenone azine. This paramagnetic product can be independently synthesized by oxidation of L^{tBu}Co with AgPF₆,^{11c} and X-ray diffraction of a single crystal revealed the product to be L^{tBu}CoPF₆, **4-Co-PF₆**. The solid state molecular structure of **4-Co-PF₆** (Figure 8) features only the second example of bidentate coordination of

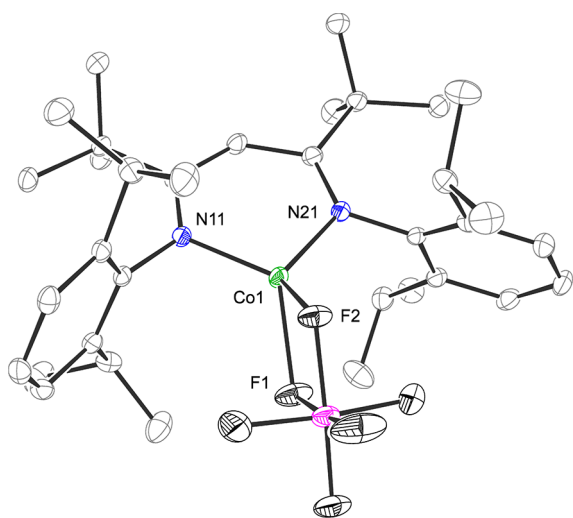


Figure 8. Molecular structure of L^{tBu}CoPF₆, **4-Co-PF₆**. Thermal ellipsoids are displayed at the 50% probability level. Hydrogen atoms are omitted for clarity. Selected bond lengths (Å) and angles (deg): Co1–N11 1.914(1), Co1–N21 1.913(1), Co1–F1 2.0794(8), Co1–F2 2.0843(8); N11–Co1–N21 99.96(4), F1–Co1–F2 65.16(3).

hexafluorophosphate to a transition metal.³¹ The solution magnetic moment of 4.6(1) μ_B for **4-Co-PF₆** is consistent with high spin cobalt(II), falling within error of the solution magnetic moment of the three-coordinate cobalt(II) (*S* = 3/2 ground state) complex L^{tBu}CoCl.^{11a} The coordination of the PF₆ anion is fluxional, as a second structure measured of crystals grown from diethyl ether revealed the PF₆ anion binding in a monodentate fashion under these conditions, with a fourth coordination site occupied by diethyl ether (**4-Co-PF₆(OEt₂)**); see Supporting Information, Figure S22).

Intrigued by our observation of benzophenone azine formation in oxidations of **1-Fe** and **1-Co**, we subsequently explored the catalytic activity of L^{tBu}FeOTf and **4-Co-PF₆** toward the conversion of diphenyldiazomethane to benzophenone azine. While preliminary investigations into the iron system gave multiple unidentified products in addition to benzophenone azine, 10 mol % loading of **4-Co-PF₆** in benzene catalyzed the conversion of diphenyldiazomethane to benzophenone azine as the only organic product in 54% yield after 4 h at room temperature. In the absence of added catalyst, diphenyldiazomethane yielded benzophenone azine in <5% yield under the same conditions. In order for catalysis to occur, a vacant coordination site is necessary at the metal center and the PF₆ anion is presumably sufficiently labile for this to occur. Catalytic decomposition of diphenyldiazomethane to benzophenone azine by the Lewis acidic complex [CpFe(CO)₂(THF)](BF₄) has been reported.³² Given the availability of an open coordination site in **4-Co-PF₆** following dissociation of a coordinated F, it is reasonable to suggest that **4-Co-PF₆** catalyzes diazoalkane decomposition by a mechanism that proceeds via a cobalt carbene intermediate. This reactivity contrasts with the previously reported reaction of **4-Fe-BAr^F₄** with ethyl diazoacetate, which resulted in electrophilic attack of the central position of the β-diketiminate by the diazo nitrogen after coordination by the carbonyl oxygen to the metal center.³³

■ COMPUTATIONAL STUDIES

To complement the computational studies that had been performed previously on **1-Co**, the new compounds **1-Fe**, **2-Co** and **3-Co** were investigated using Density Functional Theory (DFT). In accordance with the experimentally determined magnetic moment of **1-Fe**, optimization of **1-Fe** as a high-spin (*S* = 3/2) system resulted in a lower energy and an optimized structure that agreed better with the experimentally determined solid-state structure (see Table 1) than the corresponding low spin (*S* = 1/2) optimization. Compounds **2-Co** (*S* = 1/2) and **3-Co** (*S* = 1/2) were also optimized using the indicated spin states, based on the experimentally determined magnetic moments, and yielded geometries that were in reasonable agreement with the structure determined by X-ray crystallography. As with the previous studies on **1-Co**, the M06L/B1 functional and basis set (see Experimental Section for description of the basis sets) consistently gave geometries that were in better agreement with the experimentally determined structures than either ωB97xD/B1 or PBE0/B1 (see Table 1 for comparison of select metrical parameters).²⁰

There is a tendency for the M–N bond lengths to be slightly overestimated in the calculated structures of **1–3**, as is often observed in transition metal systems.³⁴ Though this is most pronounced in **3-Co-DFT**, the predicted bond lengths are within good agreement of those determined experimentally. There is no evidence of systematic over/underestimation of the bond lengths within the ligands, and all are within good

agreement of the experimentally determined values. The experimentally validated geometries, **1-Fe-DFT**, **2-Co-DFT** and **3-Co-DFT**, were therefore used for all further computational studies (we distinguish the calculated geometries from those determined experimentally with the DFT suffix).

The electronic structures of **1-Fe-DFT**, **2-Co-DFT**, and **3-Co-DFT** were subsequently investigated using the hybrid functional M06/B2 (see [Experimental Section](#) for description). Frontier molecular orbital diagrams for **1-Fe-DFT** ([Figure S25](#)), **2-Co-DFT** ([Figure S26](#)) and **3-Co-DFT** ([Figure S27](#)) are included in the [Supporting Information](#). Maximally aligning the α - and β -spin electrons indicated that **1-Fe-DFT** and **3-Co-DFT** contain ligand based radicals (overlap between corresponding orbital pair 62% and 66%, respectively; see [Figure 9](#)).

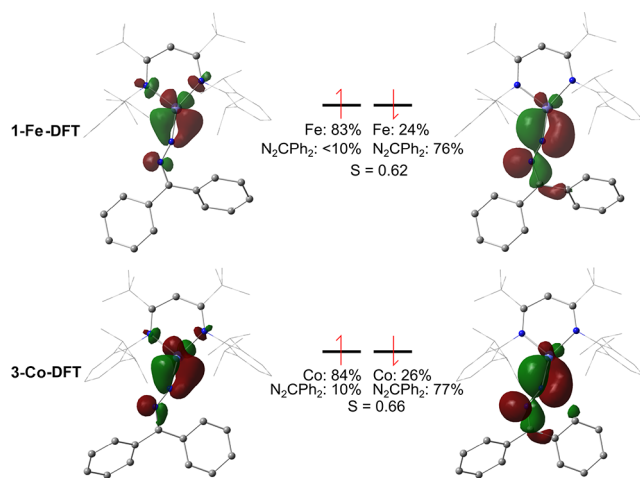


Figure 9. Spin polarized orbitals in the qualitative MO diagram of **1-Fe-DFT** and **3-Co-DFT** that come from maximally aligning the α - and β -spin orbitals. Surfaces are depicted with an isovalue of 0.04 au S represents the overlap integral between the correlated α - and β -spin electrons; all other overlaps were greater than 0.97. Other frontier orbitals are shown in the [Supporting Information](#).

The AO contributions to the corresponding pairs in **1-Fe-DFT** and **3-Co-DFT** clearly show that the α -spin orbital is metal based (83% and 84%, respectively) while the β -spin orbital is located on the diazoalkane moiety (76% and 77%, respectively). Broken symmetry calculations, as developed by Noodleman,³⁵ were performed on these two compounds, and converged to match the unrestricted calculation. Spin density plots of **1-Fe-DFT**, **1-Co-DFT** and **3-Co-DFT** are almost indistinguishable from each other and feature significant β -spin density on the NNC unit of the diazoalkane ligand (for **1-Fe-DFT** see [Figure 10](#); for **1-Co-DFT** and **3-Co-DFT** see [Supporting Information Figures S28 and S29](#), respectively).

Natural Bond Order (NBO) studies continue to grow in popularity, because they provide a way to correlate canonical molecular orbitals with Lewis structures, a description of bonding that is more familiar to chemists.³⁶ Furthermore, they provide an impartial assessment of bond order, both through the Lewis structure description they generate, and Wiberg Bond Indices (WBIs). For the unrestricted calculations described here, the different Lewis structures for different spins approach (DLDS) was used.³⁷ Due to the requirements of the NBO program, a basis set without diffuse functionals, B3, was used (see experimental details). The NBO analysis of **1-Fe-DFT** and **3-Co-DFT** is consistent with an anionic diazoalkane ligand

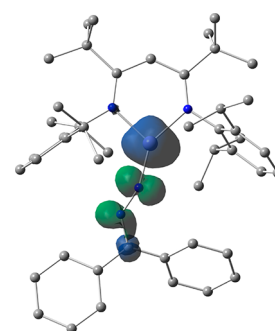


Figure 10. Spin-density plot of **1-Fe-DFT**. Surfaces depicted with an isovalue of 0.01 au. Color coded: α -spin, blue; β -spin, green.

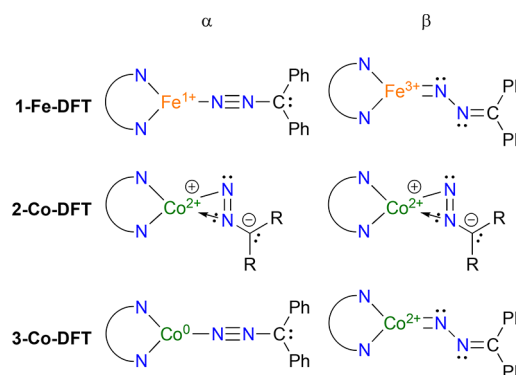


Figure 11. Resonance structures that correspond to the NBO-determined single electron α - and β -spin orbitals for **1-Fe-DFT**, **2-Co-DFT** and **3-Co-DFT**. Two-electron Lewis structures are depicted for clarity, though these are meant to indicate the locations of single electrons. See [Figure 1](#) for common resonance structures ascribed to transition metal diazoalkane complexes.

based radical that is antiferromagnetically coupled to the transition metal center ([Figure 11](#)). This is evidenced by the extra β -spin electron on the diazoalkane moiety, and one fewer transition metal centered β -spin electron than would be expected for the formal d-electron count and spin state. In the case of **2-Co-DFT**, however, NBO analysis suggests that two-electron reduction of the diazoalkane has occurred, and that it is now best described as a dianionic ligand ([Figure 11](#)). This assignment is consistent with the longer N–N and N–C bonds in the molecular structure of **2-Co**, relative to the terminally bound compounds **1-Fe** and **1-Co**. WBIs are consistent with the description of all compounds reported herein based on spectroscopic and computational studies (see [Supporting Information, Figure S30](#)).

DISCUSSION

Periodic Trends in Formation and Structures of Diazoalkane Complexes. Diazoalkane complexes **1-3** cover formal oxidation states 0–I and d-electron counts of 7–9 at the iron and cobalt atoms. The iron(II) and cobalt(II) d^6 and d^7 complexes, $L^{tBu}Fe(OTf)$ and **4-Co-PF₆**, which result from oxidation of the formally iron(I) and cobalt(I) precursors **1-Co** and **1-Fe**, did not form stable complexes with diphenyldiazoalkane. All complexes have been characterized structurally, spectroscopically and by computational methods either in this study or previously.^{10,29} On the basis of X-ray diffraction studies, magnetic moment, EPR spectroscopy, and DFT studies, **1-Fe**, **1-Co** and **3-Co** feature a diazoalkane radical

anion antiferromagnetically coupled to the transition metal center. Ligand noninnocence of this type can be difficult to distinguish spectroscopically, but the nonlinear geometry of the diazoalkane ligand in all complexes strongly implicates anion character on the diazoalkane. The magnetic moment indicates that any radical character on the ligand is antiferromagnetically coupled to the metal center, and this is supported by the spin-unrestricted DFT calculations. Furthermore, these computational studies suggest that resonance structures I and IV best describe the α - and β -spin electrons, respectively (Figure 1), as part of the different Lewis structures for different spins approach (DLDS).³⁶ The extra β -spin on the diazoalkane in this valence-bond description corresponds to the radical anion character in the molecular-orbital picture. Although these systems are charge separated, the DFT calculations indicate strong coupling between the corresponding pair of α - and β -electrons (calculated J for 1-Fe, -629 cm^{-1} ; 1-Co, -909 cm^{-1} ; 3-Co, -806 cm^{-1}). Radical character of this type is rarely assigned in diazoalkane complexes, but not unprecedented,⁹ and a reversible diazoalkane radical coupling reaction has been reported.³⁸

The electronic flexibility of the diazoalkane is demonstrated by 2-Fe and 2-Co, in which the diazoalkane isomerizes to an η^2 - N,N' mode that is reduced by two electrons as shown by structural, spectroscopic, and for 2-Co, DFT studies. DFT studies suggest that resonance structure V best describes both the α - and β -spin electrons of the η^2 - N,N' bound diazoalkane (Figure 1). This is consistent with previously reported side-on bound diazoalkane complexes.¹⁴ The increase in diazoalkane reduction is reasonable given the greater overlap between the d-orbitals of the metal centers and the π^* antibonding orbitals of the diazoalkane ligand.³⁹ Comparison of 2-Co and 3-Co, in which the formal oxidation state of the cobalt atom is the same, shows that the change in geometry correlates with the increased charge movement to the diazoalkane.

The coordination of the potassium ion in 2-Fe and 2-Co to the terminal nitrogen atom of the diazoalkane warrants further discussion. With the exception of transition metal complexes in which the diazoalkane ligand bridges between identical metal centers (e.g., $\text{Cp}(\text{Cl})\text{Ti}(\mu\text{-}\eta^2\text{:}\eta^1\text{-N}_2\text{CPh}_2)_2\text{Ti}(\text{Cl})\text{Cp}$, $(\mu\text{-}\eta^5\text{:}\eta^5\text{-C}_{10}\text{H}_8)\text{Zr}_2(\mu\text{-}\eta^2\text{:}\eta^1\text{-N}_2\text{CPh}_2)\text{Cl}_2\text{Cp}_2$),^{28b,40} there is only one example in the literature in which a diazoalkane ligand is also coordinated to a Lewis acid, $\text{Cp}^*\text{Ti}\{\mu\text{-}\eta^2\text{:}\eta^1\text{-N}_2\text{C}(\text{H})(p\text{-tol})\}\cdot\text{AlNp}_3$ (Np = neopentyl). However, this titanium diazoalkane complex adopted η^2 - N,N' binding modes with or without the Lewis acid. Our system is thus the first crystallographically and spectroscopically characterized example of a Lewis acid induced change in coordination mode of a diazoalkane transition metal complex. The fact that this change is caused by the potassium cation, not by a change in oxidation state, is shown by reversion to the terminally bound diazoalkane structure after the potassium is sequestered by a crown ether. Potassium sequestration by crown ether in 3-Co (in which there is no change in formal oxidation state from 2-Co) induces the diazoalkane to revert back to radical anion character.

Catalytic Formation of Azine and a Cobalt Carbene.

The cobalt(II), d^7 complex 4-Co-PF₆ catalyzes the conversion of diphenyldiazomethane to benzophenone azine. The iron(II) complex $[\text{CpFe}(\text{CO})_2(\text{THF})][\text{BF}_4]$, reported by Bennett and co-workers, has previously been shown to afford the same transformation with 10 mol % catalyst loading.³² In addition to benzophenone azine (yield = 39%), tetraphenylacetylene was

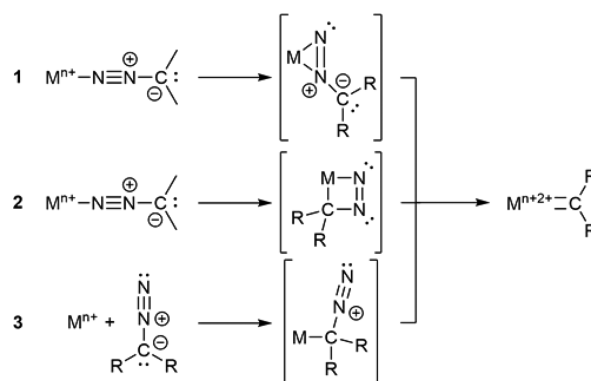


Figure 12. Possible mechanisms of carbene formation.

also isolated (26%). They used the isolated products to suggest a mechanism that has an iron(IV) carbene intermediate. It is reasonable that an analogous mechanism is effective in the diketiminate system described here, and, given the identical ligand environments used in the current study, clearly shows that steric effects alone do not prevent carbene formation in 1–3.

The mechanism of azine formation in the current system is unclear, though it presumably proceeds through a carbene intermediate. Reasonable monometallic mechanisms for carbene formation include the following (Figure 12). (1) Initial N-bound adduct formation by the diazoalkane that then "slips" to C-bound, followed by N_2 loss. (2) Initial N-bound adduct formation that subsequently forms a heterocycle following the formation of a M–C bond, which then leads to N_2 loss (the analogous mechanism is believed to be active in the conversion of organic azides to imido complexes).⁴¹ (3) Direct formation of a M–C bond, followed by N_2 elimination.

A detailed study by Milstein and co-workers on a rhodium system elucidated the importance of steric effects on carbene formation.⁴² They favored mechanism 3 (above), in which η^1 -C binding leads to a carbene containing compound, whereas initial N-bound complex formation (which is the kinetic product in sterically encumbered systems) was deleterious. Chirik and co-workers have also demonstrated a similar effect where decreasing the steric bulk of the ligands enabled carbene formation.^{4h} As all of the complexes discussed in this article have the same supporting ligand, the tendency of the lower oxidation state complexes to form stable adducts (1-Fe, 1-Co, and 3-Co) relative to the iron(II) and cobalt(II) compounds ($L^{\text{tBu}}\text{Fe}(\text{OTf})$ and 4-Co-PF₆) suggests that electronic factors also play an important role.

In our system, it may seem surprising that the more highly reduced complexes are less prone to generate carbene intermediates with formal oxidation at the metal center, while the cobalt complex with the lowest d-electron count is the one that gives evidence for carbene formation. We surmise that in the low-coordinate, low-valent systems used here, end-on binding gives strong overlap between high-lying, filled metal d-orbitals and diazoalkane π^* -orbitals, leading to charge buildup on the diazoalkane and strengthening of the M–N and C–N bonds that prevents N_2 loss. The higher oxidation state compounds, on the other hand, do not have analogous charge transfer and can lose N_2 .

CONCLUSIONS

Structural and computational characterization of new diazoalkane complexes of iron and cobalt demonstrates the noninnocent nature of the diazoalkane. This easily reduced ligand can accommodate one or two electrons from the metal, and the extent of charge transfer depends not only on the oxidation level of the metal, but also on the presence of potassium ions that encourage an η^2 binding mode. These insights can potentially be used to control the binding mode and charge transfer to other diazoalkane adducts that are precursors to carbene complexes.

ASSOCIATED CONTENT

Supporting Information

The Supporting Information is available free of charge on the ACS Publications website at DOI: 10.1021/acs.inorgchem.8b00468.

Spectroscopic data (PDF)

Accession Codes

CCDC 1824903–1824907 and 1824914 contain the supplementary crystallographic data for this paper. These data can be obtained free of charge via www.ccdc.cam.ac.uk/data_request/cif, or by emailing data_request@ccdc.cam.ac.uk, or by contacting The Cambridge Crystallographic Data Centre, 12 Union Road, Cambridge CB2 1EZ, UK; fax: +44 1223 336033.

AUTHOR INFORMATION

Corresponding Author

*E-mail: patrick.holland@yale.edu.

ORCID

Javier Vela: 0000-0001-5124-6893

Ryan E. Cowley: 0000-0003-1791-4266

William W. Brennessel: 0000-0001-5461-1825

Patrick L. Holland: 0000-0002-2883-2031

Present Addresses

[§](J.V.) Department of Chemistry, Iowa State University, Ames, Iowa 50010, United States.

^{||}(D.J.V.) Department of Biological Sciences, Louisiana State University, Baton Rouge, Louisiana 70803, United States.

Funding

Funding was provided by the American Australian Association (S.J.B.) and the U.S. Department of Energy, Office of Basic Energy Sciences, Grant DE-FG02–09ER16089 (P.L.H.). Analytical data were from the CENTC Elemental Analysis Facility at the University of Rochester, funded by the NSF (CHE-0650456). This work was supported in part by the facilities and staff of the Yale High Performance Computing Center, which was partially funded by the NSF (CNS 08–21132). The Advanced Light Source is supported by the Director, Office of Science, Office of Basic Energy Sciences, of the U.S. Department of Energy under Contract No. DE-AC02–05CH11231.

Notes

The authors declare no competing financial interest.

ACKNOWLEDGMENTS

Some EPR spectroscopy of 3-Co was collected at the National Biomedical Center for Advanced ESR Technology, which is supported by the National Institute of General Medical Sciences of the NIH under Award P41GM103521. We thank

Boris Dzikovski for assistance with EPR data collection. We also thank Gary Brudvig for the use of an EPR spectrometer and for helpful discussions. Some crystallography was performed at the Advanced Light Source (ALS), which is supported by the Director, Office of Science, Office of Basic Energy Sciences, of the U.S. Department of Energy under Contract No. DE-AC02-05CH11231.

REFERENCES

- (1) (a) Herrmann, W. A. Organometallic Syntheses with Diazoalkanes. *Angew. Chem., Int. Ed. Engl.* **1978**, *17*, 800–812. (b) Sutton, D. Organometallic Diazo Compounds. *Chem. Rev.* **1993**, *93*, 995–1022. (c) Mizobe, Y.; Ishii, Y.; Hidai, M. Synthesis and reactivities of diazoalkane complexes. *Coord. Chem. Rev.* **1995**, *139*, 281–311. (d) Dartiguenave, M.; Menu, M. J.; Deydier, E.; Dartiguenave, Y.; Siebald, H. Crystal and molecular structures of transition metal complexes with N- and C-bonded diazoalkane ligands. *Coord. Chem. Rev.* **1998**, *178–180*, 623–663. (e) Poverenov, E.; Leitus, G.; Shimon, L. J. W.; Milstein, D. C-Metalated Diazoalkane Complexes of Platinum Based on PCP- and PCN-Type Ligands. *Organometallics* **2005**, *24*, 5937–5944. (f) Samant, R. G.; Graham, T. W.; Rowsell, B. D.; McDonald, R.; Cowie, M. Coordination and Activation of Diazoalkanes in the Presence of Rh/Ru and Rh/Os Metal Combinations. *Organometallics* **2008**, *27*, 3070–3081.
- (2) Selected first-row examples: (a) Clegg, W.; Chew, K. C.; Coles, M. P.; Elsegood, M. R. J.; Gibson, V. C.; White, A. J. P.; Williams, D. J. Synthesis and Characterisation of 2,6-Diisopropylphenylimido Complexes of Chromium in Oxidation States IV–VI. *J. Chem. Soc., Dalton Trans.* **1999**, 2633–2640. (b) Castellano, B.; Solari, E.; Floriani, C.; Scopelliti, R.; Re, N. Reactivity of a Vanadium(III) Center over an Oxo Surface Modeled by Calix[4]arene. *Inorg. Chem.* **1999**, *38*, 3406–3413. (c) Jenkins, D. M.; Betley, T. A.; Peters, J. C. Oxidative Group Transfer to Co(I) Affords a Terminal Co(III) Imido Complex. *J. Am. Chem. Soc.* **2002**, *124*, 11238–11239. (d) Sydora, O. L.; Kuiper, D. S.; Wolczanski, P. T.; Lobkovsky, E. B.; Dinescu, A.; Cundari, T. R. The Butterfly Dimer [^tBu₃SiO)Cr]₂(μ-Os^tBu₃)₂ and its Oxidative Cleavage to (^tBu₃SiO)₂Cr(=N–N=CPh₃)₂ and (^tBu₃SiO)₂Cr=N(2,6-Ph₂-C₆H₃). *Inorg. Chem.* **2006**, *45*, 2008–2021. (e) Bart, S. C.; Bowman, A. C.; Lobkovsky, E.; Chirik, P. J. Iron Diazoalkane Chemistry: N–N Bond Hydrogenation and Intramolecular C–H Activation. *J. Am. Chem. Soc.* **2007**, *129*, 7212–7213. (f) Herbert, D. E.; Lara, N. C.; Agapie, T. Arene C–H Amination at Nickel in Terphenyl-Diphosphine Complexes with Labile Metal–Arene Interactions. *Chem. - Eur. J.* **2013**, *19*, 16453–16460. (g) Tiong, P. J.; Groom, L. R.; Clot, E.; Mountford, P. Synthesis, Bonding and Reactivity of a Terminal Titanium Alkylidene Hydrazido Compound. *Chem. - Eur. J.* **2013**, *19*, 4198–4216.
- (3) de Frémont, P.; Marion, N.; Nolan, S. P. Carbenes: Synthesis, properties, and organometallic chemistry. *Coord. Chem. Rev.* **2009**, *253*, 862–892.
- (4) Selected first-row examples synthesized from diazoalkanes: (a) Herrmann, W. A.; Plank, J.; Kriechbaum, G. W.; Ziegler, M. L.; Pfisterer, H.; Atwood, J. L.; Rogers, R. D. Komplexchemie reaktiver organischer Verbindungen XLVII. Synthese, Strukturchemie und Druckcarbonylierung von Metallcarben-Komplexen. *J. Organomet. Chem.* **1984**, *264*, 327–352. (b) Herrmann, W. A.; Hubbard, J. L.; Bernal, L.; Korp, J. D.; Haymore, B. L.; Hillhouse, G. L. Complex chemistry of reactive organic compounds. 46. Conformation of metal carbene complexes: synthesis and structure of carbonyl(η^5 -cyclopentadienyl)(diphenylcarbene)nitrosylchromium and its relationship to the isoelectronic compound dicarbonyl(η^5 -cyclopentadienyl)-(diphenylcarbene)manganese. *Inorg. Chem.* **1984**, *23*, 2978–2983. (c) Klose, A.; Solari, E.; Floriani, C.; Re, N.; Chiesi-Villa, A.; Rizzoli, C. Iron–carbene functionalities supported by a macrocyclic ligand: iron–carbon double bond stabilized by tetramethyldibenzotetraazaannulene. *Chem. Commun.* **1997**, 2297–2298. (d) Li, Y.; Huang, J. S.; Zhou, Z. Y.; Che, C. M.; You, X. Z. Remarkably Stable Iron Porphyrins Bearing Nonheteroatom-Stabilized Carbene or (Alkoxy carbonyl)carbenes:

Isolation, X-ray Crystal Structures, and Carbon Atom Transfer Reactions with Hydrocarbons. *J. Am. Chem. Soc.* **2002**, *124*, 13185–13193. (e) Dai, X.; Warren, T. H. Discrete Bridging and Terminal Copper Carbenes in Copper-Catalyzed Cyclopropanation. *J. Am. Chem. Soc.* **2004**, *126*, 10085–10094. (f) Hofmann, P.; Shishkov, I. V.; Rominger, F. Synthesis, Molecular Structures, and Reactivity of Mono- and Binuclear Neutral Copper(I) Carbenes. *Inorg. Chem.* **2008**, *47*, 11755–11762. (g) Shishkov, I. V.; Rominger, F.; Hofmann, P. Remarkably Stable Copper(I) α -Carbonyl Carbenes: Synthesis, Structure, and Mechanistic Studies of Alkene Cyclopropanation Reactions. *Organometallics* **2009**, *28*, 1049–1059. (h) Russell, S. K.; Hoyt, J. M.; Bart, S. C.; Milsmann, C.; Stieber, S. C. E.; Semproni, S. P.; DeBeer, S.; Chirik, P. J. Synthesis, electronic structure and reactivity of bis(imino)pyridine iron carbene complexes: evidence for a carbene radical. *Chem. Sci.* **2014**, *5*, 1168–1174. (i) Bellow, J. A.; Stoian, S. A.; van Tol, J.; Ozarowski, A.; Lord, R. L.; Groysman, S. Synthesis and Characterization of a Stable High-Valent Cobalt Carbene Complex. *J. Am. Chem. Soc.* **2016**, *138*, 5531–5534.

(5) Selected examples: (a) Messerle, L.; Curtis, M. D. Reaction of diaryldiazomethanes with a metal-metal triple bond: synthesis, structural characterizations, and reactivity of novel bridging diazoalkane and alkylidene complexes. *J. Am. Chem. Soc.* **1980**, *102*, 7789–7791. (b) Mindiola, D. J.; Hillhouse, G. L. Synthesis, Structure, and Reactions of a Three-Coordinate Nickel-Carbene Complex, {1,2-Bis(di-*tert*-butylphosphino)ethane}NiCPh₂. *J. Am. Chem. Soc.* **2002**, *124*, 9976–9977. (c) Cohen, R.; Rybtchinski, B.; Gandelman, M.; Rozenberg, H.; Martin, J. M. L.; Milstein, D. Metallocarbenes from Diazoalkanes: An Experimental and Computational Study of the Reaction Mechanism. *J. Am. Chem. Soc.* **2003**, *125*, 6532–6546. (d) Iluc, V. M.; Hillhouse, G. L. Three-Coordinate Nickel Carbene Complexes and Their One-Electron Oxidation Products. *J. Am. Chem. Soc.* **2014**, *136*, 6479–6488.

(6) Selected first-row examples: (a) Penoni, A.; Wanke, R.; Tollari, S.; Gallo, E.; Musella, D.; Ragaini, F.; Demartin, F.; Cenini, S. Cyclopropanation of Olefins with Diazoalkanes, Catalyzed by Co^{II}(porphyrin) Complexes – A Synthetic and Mechanistic Investigation and the Molecular Structure of Co^{III}(TPP)(CH₂CO₂Et) (TPP = Dianion of *meso*-Tetraphenylporphyrin). *Eur. J. Inorg. Chem.* **2003**, *2003*, 1452–1460. (b) Ingleson, M. J.; Pink, M.; Caulton, K. G. Reducing Power of Three-Coordinate Cobalt(I). *J. Am. Chem. Soc.* **2006**, *128*, 4248–4249. (c) Mankad, N. P.; Peters, J. C. Diazoalkanes react with a bis(phosphino)borate copper(I) source to generate [Ph₂BP^{tBu}]₂Cu(η^1 -N₂CR₂), [Ph₂BP^{tBu}]₂Cu(CPh₃), and [Ph₂BP^{tBu}]₂Cu-N(CPh₂)(NCPH₂). *Chem. Commun.* **2008**, 1061–1063. (d) Ingleson, M. J.; Pink, M.; Fan, H.; Caulton, K. G. Redox Chemistry of the Triplet Complex (PNP)Co^I. *J. Am. Chem. Soc.* **2008**, *130*, 4262–4276. (e) Xu, X.; Zhu, S.; Cui, X.; Wojtas, L.; Zhang, X. P. Cobalt(II)-Catalyzed Asymmetric Olefin Cyclopropanation with α -Ketodiazooacetates. *Angew. Chem., Int. Ed.* **2013**, *52*, 11857–11861.

(7) (a) Basuli, F.; Bailey, B. C.; Watson, L. A.; Tomaszewski, J.; Huffman, J. C.; Mindiola, D. J. Four-Coordinate Titanium Alkylidene Complexes: Synthesis, Reactivity, and Kinetic Studies Involving the Terminal Neopentylidene Functionality. *Organometallics* **2005**, *24*, 1886–1906. (b) Russell, S. K.; Lobkovsky, E.; Chirik, P. J. N–N Bond Cleavage in Diazoalkanes by a Bis(imino)pyridine Iron Complex. *J. Am. Chem. Soc.* **2009**, *131*, 36–37. (c) Kurogi, T.; Ishida, Y.; Hatanaka, T.; Kawaguchi, H. Multielectron reduction of diazoalkane and azides via reversible cyclometalation in ditantalum complexes. *Chem. Commun.* **2012**, *48*, 6809–6811. (d) Ito, J.; Crestani, M. G.; Bailey, B. C.; Gao, X.; Mindiola, D. J. N–N bond cleavage in diazoalkanes with a titanium alkylidene. *Polyhedron* **2014**, *84*, 177–181.

(8) Kauffmann, T.; Hage, S. M. Stable Free Radicals Formed by the Action of Sodium onto Diazomethane Derivatives or Phenyl Azide. *Angew. Chem., Int. Ed. Engl.* **1963**, *2*, 156.

(9) (a) Lam, O. P.; Feng, P. L.; Heinemann, F. W.; O'Connor, J. M.; Meyer, K. Charge-Separation in Uranium Diazomethane Complexes Leading to C–H Activation and Chemical Transformation. *J. Am. Chem. Soc.* **2008**, *130*, 2806–2816. (b) Sazama, G. T.; Betley, T. A.

Multiple, Disparate Redox Pathways Exhibited by a Tris(pyrrolido)-ethane Iron Complex. *Inorg. Chem.* **2014**, *53*, 269–281.

(10) Bonyhady, S. J.; Goldberg, J. M.; Wedgwood, N.; Dugan, T. R.; Eklund, A. G.; Brennessel, W. W.; Holland, P. L. Cobalt(II) Complex of a Diazoalkane Radical Anion. *Inorg. Chem.* **2015**, *54*, 5148–5150.

(11) (a) Holland, P. L.; Cundari, T. R.; Perez, L. L.; Eckert, N. A.; Lachicotte, R. J. Electronically Unsaturated Three-Coordinate Chloride and Methyl Complexes of Iron, Cobalt, and Nickel. *J. Am. Chem. Soc.* **2002**, *124*, 14416–14424. (b) Smith, J. M.; Lachicotte, R. J.; Pittard, K. A.; Cundari, T. R.; Lukat-Rodgers, G.; Rodgers, K. R.; Holland, P. L. Stepwise Reduction of Dinitrogen Bond Order by a Low-Coordinate Iron Complex. *J. Am. Chem. Soc.* **2001**, *123*, 9222–9223. (c) Dugan, T. R.; Sun, X.; Rybak-Akimova, E. V.; Olatunji-Ojo, O.; Cundari, T. R.; Holland, P. L. A Masked Two-Coordinate Cobalt(I) Complex That Activates C–F Bonds. *J. Am. Chem. Soc.* **2011**, *133*, 12418–12421. (d) Pfirrmann, S.; Limberg, C.; Herwig, C.; Stöber, R.; Ziemer, B. A Dinuclear Nickel(I) Dinitrogen Complex and its Reduction in Single-Electron Steps. *Angew. Chem., Int. Ed.* **2009**, *48*, 3357–3361. (e) Spencer, D. J. E.; Aboeella, N. W.; Reynolds, A. M.; Holland, P. L.; Tolman, W. B. β -Diketimate Ligand Backbone Structural Effects on Cu(I)/O₂ Reactivity: Unique Copper-Superoxo and Bis(μ -oxo) Complexes. *J. Am. Chem. Soc.* **2002**, *124*, 2108–2109.

(12) (a) Smith, L. I.; Howard, K. L. Diphenyldiazomethane. *Organic Syntheses* **1955**, *Coll. Vol. III*, 351–352. (b) Miller, J. B. Preparation of Crystalline Diphenyldiazomethane. *J. Org. Chem.* **1959**, *24*, 560–561. (c) Javed, M. I.; Brewer, M. Diazo Preparation via Dehydrogenation of Hydrazones with "Activated" DMSO. *Org. Lett.* **2007**, *9*, 1789–1792. (d) Javed, M. I.; Brewer, M. Diphenyldiazomethane. *Org. Synth.* **2008**, *85*, 189–195.

(13) Smith, J. M.; Sadique, A. R.; Cundari, T. R.; Rodgers, K. R.; Lukat-Rodgers, G.; Lachicotte, R. J.; Flaschenriem, C. J.; Vela, J.; Holland, P. L. Studies of Low-Coordinate Iron Dinitrogen Complexes. *J. Am. Chem. Soc.* **2006**, *128*, 756–769.

(14) Ding, K.; Pierpont, A. W.; Brennessel, W. W.; Lukat-Rodgers, G.; Rodgers, K. R.; Cundari, T. R.; Bill, E.; Holland, P. L. Cobalt-Dinitrogen Complexes with Weakened N–N Bonds. *J. Am. Chem. Soc.* **2009**, *131*, 9471–9472.

(15) Schubert, E. M. Utilizing the Evans method with a superconducting NMR spectrometer in the undergraduate laboratory. *J. Chem. Educ.* **1992**, *69*, 62.

(16) Stoll, S.; Schweiger, A. EasySpin, a comprehensive software package for spectral simulation and analysis in EPR. *J. Magn. Reson.* **2006**, *178*, 42–55.

(17) Frisch, M. J.; Trucks, G. W.; Schlegel, H. B.; Scuseria, G. E.; Robb, M. A.; Cheeseman, J. R.; Scalmani, G.; Barone, V.; Mennucci, B.; Petersson, G. A.; Nakatsuji, H.; Caricato, M.; Li, X.; Hratchian, H. P.; Izmaylov, A. F.; Bloino, J.; Zheng, G.; Sonnenberg, J. L.; Hada, M.; Ehara, M.; Toyota, K.; Fukuda, R.; Hasegawa, J.; Ishida, M.; Nakajima, T.; Honda, Y.; Kitao, O.; Nakai, H.; Vreven, T.; Montgomery, J. A. J.; Peralta, J. E.; Ogliaro, F.; Bearpark, M.; Heyd, J. J.; Brothers, E.; Kudin, K. N.; Staroverov, V. N.; Kobayashi, R.; Normand, J.; Raghavachari, K.; Rendell, A.; Burant, J. C.; Iyengar, S. S.; Tomasi, J.; Cossi, M.; Rega, N.; Millam, M. J.; Klene, M.; Knox, J. E.; Cross, J. B.; Bakken, V.; Adamo, C.; Jaramillo, J.; Gomperts, R.; Stratmann, R. E.; Yazyev, O.; Austin, A. J.; Cammi, R.; Pomelli, C.; Ochterski, J. W.; Martin, R. L.; Morokuma, K.; Zakrzewski, V. G.; Voth, G. A.; Salvador, P.; Dannenberg, J. J.; Dapprich, S.; Daniels, A. D.; Farkas, Ö.; Foresman, J. B.; Ortiz, J. V.; Cioslowski, J.; Fox, D. J. *Gaussian 09*, Revision D.01; Gaussian: Wallingford, CT, 2009.

(18) (a) Glendening, E. D.; Landis, C. R.; Weinhold, F. NBO 6.0: Natural bond orbital analysis program. *J. Comput. Chem.* **2013**, *34*, 1429. (b) Glendening, E. D.; Badenhop, J. K.; Reed, A. E.; Carpenter, J. E.; Bohmann, J. A.; Morales, C. M.; Landis, C. R.; Weinhold, F. *NBO 6.0*, Theoretical Chemistry Institute: University of Wisconsin, Madison, 2013.

(19) Grimme, S.; Antony, J.; Ehrlich, S.; Krieg, H. A consistent and accurate *ab initio* parametrization of density functional dispersion correction (DFT-D) for the 94 elements H–Pu. *J. Chem. Phys.* **2010**, *132*, 154104.

- (20) M06L: Zhao, Y.; Truhlar, D. G. A new local density functional for main-group thermochemistry, transition metal bonding, thermochemical kinetics, and noncovalent interactions. *J. Chem. Phys.* **2006**, *125*, 194101. ω B97xD: Chai, J.-D.; Head-Gordon, M. Long-range corrected hybrid density functionals with damped atom-atom dispersion corrections. *Phys. Chem. Chem. Phys.* **2008**, *10*, 6615–6620. PBE0: (a) Perdew, J. P.; Burke, K.; Ernzerhof, M. Generalized Gradient Approximation Made Simple. *Phys. Rev. Lett.* **1996**, *77*, 3865–3868. (b) Perdew, J. P.; Burke, K.; Ernzerhof, M. Errata Generalized Gradient Approximation Made Simple. *Phys. Rev. Lett.* **1997**, *78*, 1396. (c) Adamo, C.; Barone, V. Toward reliable density functional methods without adjustable parameters: The PBE0 model. *J. Chem. Phys.* **1999**, *110*, 6158–6170.
- (21) Zhao, Y.; Truhlar, D. G. The M06 suite of density functionals for main group thermochemistry, thermochemical kinetics, non-covalent interactions, excited states, and transition elements: two new functionals and systematic testing of four M06-class functionals and 12 other functionals. *Theor. Chem. Acc.* **2008**, *120*, 215–241.
- (22) (a) Smith, J. M.; Lachicotte, R. J.; Holland, P. L. N≡N Bond Cleavage by a Low-Coordinate Iron(II) Hydride Complex. *J. Am. Chem. Soc.* **2003**, *125*, 15752–15753. (b) Eckert, N. A.; Smith, J. M.; Lachicotte, R. J.; Holland, P. L. Low-Coordinate Iron(II) Amido Complexes of β -Diketiminates: Synthesis, Structure, and Reactivity. *Inorg. Chem.* **2004**, *43*, 3306–3321.
- (23) (a) Cowley, R. E.; DeYonker, N. J.; Eckert, N. A.; Cundari, T. R.; DeBeer, S.; Bill, E.; Ottenwaelder, X.; Flaschenriem, C.; Holland, P. L. Three-Coordinate Terminal Imidoiron(III) Complexes: Structure, Spectroscopy, and Mechanism of Formation. *Inorg. Chem.* **2010**, *49*, 6172–6187. (b) Cowley, R. E.; Holland, P. L. Ligand Effects on Hydrogen Atom Transfer from Hydrocarbons to Three-Coordinate Iron Imides. *Inorg. Chem.* **2012**, *51*, 8352–8361.
- (24) Stoian, S. A.; Vela, J.; Smith, J. M.; Sadique, A. R.; Holland, P. L.; Münck, E.; Bominaar, E. L. Mössbauer and Computational Study of an N_2 -Bridged Diiron Diketimate Complex: Parallel Alignment of the Iron Spins by Direct Antiferromagnetic Exchange with Activated Dinitrogen. *J. Am. Chem. Soc.* **2006**, *128*, 10181–10192.
- (25) (a) Pyykkö, P.; Atsumi, M. Molecular Single-Bond Covalent Radii for Elements 1–118. *Chem. - Eur. J.* **2009**, *15*, 186–197. (b) Pyykkö, P.; Atsumi, M. Molecular Double-Bond Covalent Radii for Elements Li-E112. *Chem. - Eur. J.* **2009**, *15*, 12770–12779.
- (26) (a) Kromm, K.; Hampel, F.; Gladysz, J. A. A New Family of Chelating Diphosphines with Transition-Metal and Carbon Stereocenters in the Backbone: A Second-Generation Rhenium-Containing System. *Organometallics* **2002**, *21*, 4264–4274. (b) Malecki, J. G.; Gryca, I.; Penkala, M. Aryldiazenido ruthenium(II) complexes. Structure and characterization of *p*-tolylidiazenido ruthenium(II) complexes with pyrazole and imidazole ligands. *Polyhedron* **2013**, *51*, 102–110.
- (27) Suturina, E. A.; Nehrkor, J.; Zadrozny, J. M.; Liu, J.; Atanasov, M.; Weyhermüller, T.; Maganas, D.; Hill, S.; Schnegg, A.; Bill, E.; Long, J. R.; Neese, F. Magneto-structural correlations in pseudotetraahedral forms of the $[Co(SPh)_4]^{2-}$ complex probed by magnetometry, MCD spectroscopy, advanced EPR techniques, and ab initio electronic structure calculations. *Inorg. Chem.* **2017**, *56*, 3102–3118.
- (28) (a) Nakamura, A.; Yoshida, T.; Cowie, M.; Otsuka, S.; Ibers, J. A. Cyclopropanation reactions of diazoalkanes with substituted olefins in the presence and absence of nickel(0) and palladium(0) catalysts. The structure of (diazofluorene)bis(*tert*-butyl isocyanide)nickel(0); a complex containing a π -bonded diazofluorene. *J. Am. Chem. Soc.* **1977**, *99*, 2108–2117. (b) Gambarotta, S.; Floriani, C.; Chiesi-Villa, A.; Guastini, C. Cyclopentadienyldichlorotitanium(III): a free-radical-like reagent for reducing azo (N:N) multiple bonds in azo and diazo compounds. *J. Am. Chem. Soc.* **1983**, *105*, 7295–7301. (c) Klein, H.; Ellrich, K.; Hammerschmitt, B.; Koch, U.; Cordier, G. Z. Coordination of Diazo Compounds to Cobalt(I) Centres, Structure of Methyl-(diazocyclopentadiene)tris(trimethylphosphane)cobalt. *Z. Naturforsch., B: J. Chem. Sci.* **1990**, *45*, 1291–1303. (d) Polse, J. L.; Andersen, R. A.; Bergman, R. G. Synthesis, Structure, and Reactivity Studies of an η^2-N_2 -Titanium Diazoalkane Complex. Generation and Trapping of a Carbene Complex Intermediate. *J. Am. Chem. Soc.* **1996**, *118*, 8737–8738. (e) Kaplan, A. W.; Polse, J. L.; Ball, G. E.; Andersen, R. A.; Bergman, R. G. Synthesis, Structure, and Reactivity of η^2-N_2 -Aryldiazoalkane Titanium Complexes: Cleavage of the N–N Bond. *J. Am. Chem. Soc.* **1998**, *120*, 11649–11662. (f) Schaub, T.; Radius, U. Z. A Stable η^2 -Bonded Diazoalkane Complex. *Z. Anorg. Allg. Chem.* **2007**, *633*, 2168–2172.
- (29) Koritsanszky, T.; Buschmann, J.; Luger, P.; Knöchel, A.; Patz, M. Experimental Charge Density Study on an Ionic Crown Ether Complex: $[Kc18-Crown-6]^+N_3^- \cdot H_2O$. *J. Am. Chem. Soc.* **1994**, *116*, 6748–6756.
- (30) Vela, J.; Cirera, J.; Smith, J. M.; Lachicotte, R. J.; Flaschenriem, C. J.; Alvarez, S.; Holland, P. L. Quantitative Geometric Descriptions of the Belt Iron Atoms of the Iron-Molybdenum Cofactor of Nitrogenase and Synthetic Iron(II) Model Complexes. *Inorg. Chem.* **2007**, *46*, 60–71.
- (31) Yamamoto, Y.; Aoki, K.; Yamazaki, H. Steric effects of ligands in silver(I) isocyanide complexes. Structure of $Ag(2,4,6-t-Bu_3C_6H_2NC)_2(PF_6)_2$ containing a bidentate PF_6 ligand. *Inorg. Chim. Acta* **1983**, *68*, 75–78.
- (32) Saha, A. K.; Hossain, M. M.; Grubisha, D. S.; Bennett, D. W. Crystal and molecular structure of benzophenone azine: evidence for an Fe(II) carbene intermediate. *J. Chem. Crystallogr.* **1995**, *25*, 383–387.
- (33) Gregory, E. A.; Lachicotte, R. J.; Holland, P. L. A Cationic Three-Coordinate Iron(II) Complex and the Reaction of β -Diketimate with Ethyl Diazoacetate. *Organometallics* **2005**, *24*, 1803–1805.
- (34) Minenkov, Y.; Singstad, Å.; Occhipinti, G.; Jensen, V. R. The accuracy of DFT-optimized geometries of functional transition metal compounds: a validation study of catalysts for olefin metathesis and other reaction in the homogeneous phase. *Dalton Trans.* **2012**, *41*, 5526–5541.
- (35) (a) Noodleman, L. Valence bond description of antiferromagnetic coupling in transition metal dimers. *J. Chem. Phys.* **1981**, *74*, 5737–5743. (b) Noodleman, L.; Davidson, E. R. Ligand spin polarization and antiferromagnetic coupling in transition metals. *Chem. Phys.* **1986**, *109*, 131–143. (c) Noodleman, L.; Peng, C. Y.; Case, D. A.; Mouesca, J.-M. Orbital interactions, electron delocalization and spin coupling in iron-sulfur clusters. *Coord. Chem. Rev.* **1995**, *144*, 199–244. (d) Lledós, A.; Moreno-Mañas, M.; Sodupe, M.; Vallribera, A.; Mata, I.; Martínez, B.; Molins, E. Bent and Linear Forms of the $(\mu-oxo)bis[trichloroferrate(III)]$ Dianion: An Intermolecular Effect - Structural, Electronic and Magnetic Properties. *Eur. J. Inorg. Chem.* **2003**, *2003*, 4187–4194.
- (36) Landis, C. R.; Weinhold, F. In *The Chemical Bond: Fundamental Aspects of Chemical Bonding*; Frenking, G.; Shaik, S., Eds.; Wiley, 2014; pp 91–120.
- (37) Carpenter, J. E.; Weinhold, F. Analysis of the geometry of the hydroxymethyl radical by the “different hybrids for different spins” natural bond orbital procedure. *J. Mol. Struct.: THEOCHEM* **1988**, *169*, 41–62.
- (38) Curley, J. J.; Murahashi, T.; Cummins, C. C. Synthesis and Reversible Reductive Coupling of Cationic, Dinitrogen-Derived Diazoalkane Complexes. *Inorg. Chem.* **2009**, *48*, 7181–7193.
- (39) Holland, P. L. Metal-dioxygen and metal-dinitrogen complexes: where are the electrons? *Dalton Trans.* **2010**, *39*, 5415–54525.
- (40) Herrmann, W. A.; Menjon, B.; Herdtweck, E. Chemistry of oxophilic transition metals. 4. Reactivity of the organozirconium(III) complex $(\mu-\eta^5-\eta^5-C_{10}H_8)[(\mu-Cl)Zr(\eta^5-C_5H_5)_2]$ with diphenyldiazo-methane, *tert*-butyl isocyanide, and trimethylsilyl azide: diazo, cyano, and imido complexes. *Organometallics* **1991**, *10*, 2134–2141.
- (41) Proulx, G.; Bergman, R. G. Synthesis, Structures, and Kinetics and Mechanism of Decomposition of Terminal Metal Azide Complexes: Isolated Intermediates in the Formation of Imidometal Complexes from Organic Azides. *Organometallics* **1996**, *15*, 684–692.
- (42) Cohen, R.; Rybtchinski, B.; Gandelman, M.; Rozenberg, H.; Martin, J. M. L.; Milstein, D. Metallocarbenes from Diazoalkanes: An

Experimental and Computational Study of the Reaction Mechanism. *J. Am. Chem. Soc.* **2003**, *125*, 6532–6546.